Atomic force microscopy study of the metal surface during a palladium-catalyzed hydrogenation membrane reaction

by

Jared C. Carson

B.S., University of New Hampshire, 2014

An Abstract of a Dissertation

submitted in partial fulfillment of the requirements for the degree

Doctor of Philosophy

Department of Chemical Engineering
College of Engineering

Kansas State University
Manhattan, Kansas

2018

Abstract

Characterizing a catalytic metal surface during heterogeneous hydrogenation is an enabling area of catalysis research. Available technology, however, often requires ultra-high vacuum or other limiting conditions which prohibit in operando research. Atomic force microscopy (AFM) can provide direct observations of fluid/solid interfaces at atmospheric conditions and in real time. Tapping-mode AFM can examine chemical and physical phenomena on surfaces in addition to topography. The work here describes using phase-angle information from tapping-mode AFM to observe liquid/solid interfaces in real time during the hydrogenation of styrene. Through optimized tuning and scanning procedures, it was possible to observe the onset of hydrogenation on the surface of palladium immersed in liquid in real time and with the topographic resolution inherent to AFM. This opens new avenues for in operando research on heterogeneous catalysis, a field that is of great fundamental and industrial importance.

For reference, a catalytic membrane reactor (CMR) was used to observe the hydrogenation of phenylacetylene over a palladium layer as a batch process. It was determined that with a H_2 diffusion rate of $3.7 \cdot 10^{-9}$ mol/s and a theoretical, calculated H_2 demand of at least $2.3 \cdot 10^{-7}$ mol/s, the reaction would be hydrogen starved and would not progress at a realistic timescale for observation by AFM. By instead using either ethylbenzene (EB) or styrene (St) as the liquid in a solvent-free approach and injecting a small volume of the other liquid into the system mid-scan, the effects of changes in chemistry on tip-surface interactions were observable. EB injections in both EB and St-immersed scans showed no significant change in phase angle. Injecting St into an EB-immersed scan environment, however, caused an increase in phase which remained relatively constant for the remaining duration of the scan, demonstrating for the first time that a liquid-phase hydrogenation reaction can be observed in operando through the phase shift of tapping mode AFM.

Atomic force microscopy study of the metal surface during a palladium-catalyzed hydrogenation membrane reaction

by

Jared C. Carson

B.S., University of New Hampshire, 2014

A Dissertation

submitted in partial fulfillment of the requirements for the degree

Doctor of Philosophy

Department of Chemical Engineering
College of Engineering

Kansas State University
Manhattan, Kansas

2018

Approved by:

Major Professor
Dr. Mary E. Rezac

Copyright

Abstract

Characterizing a catalytic metal surface during heterogeneous hydrogenation is an enabling area of catalysis research. Available technology, however, often requires ultra-high vacuum or other limiting conditions which prohibit in operando research. Atomic force microscopy (AFM) can provide direct observations of fluid/solid interfaces at atmospheric conditions and in real time. Tapping-mode AFM can examine chemical and physical phenomena on surfaces in addition to topography. The work here describes using phase-angle information from tapping-mode AFM to observe liquid/solid interfaces in real time during the hydrogenation of styrene. Through optimized tuning and scanning procedures, it was possible to observe the onset of hydrogenation on the surface of palladium immersed in liquid in real time and with the topographic resolution inherent to AFM. This opens new avenues for in operando research on heterogeneous catalysis, a field that is of great fundamental and industrial importance.

For reference, a catalytic membrane reactor (CMR) was used to observe the hydrogenation of phenylacetylene over a palladium layer as a batch process. It was determined that with a H_2 diffusion rate of $3.7 \cdot 10^{-9}$ mol/s and a theoretical, calculated H_2 demand of at least $2.3 \cdot 10^{-7}$ mol/s, the reaction would be hydrogen starved and would not progress at a realistic timescale for observation by AFM. By instead using either ethylbenzene (EB) or styrene (St) as the liquid in a solvent-free approach and injecting a small volume of the other liquid into the system mid-scan, the effects of changes in chemistry on tip-surface interactions were observable. EB injections in both EB and St-immersed scans showed no significant change in phase angle. Injecting St into an EB-immersed scan environment, however, caused an increase in phase which remained relatively constant for the remaining duration of the scan, demonstrating for the first time that a liquid-phase hydrogenation reaction can be observed in operando through the phase shift of tapping mode AFM.

Table of Contents

List of Figures

List of Tables

Acknowledgements

I must first and foremost thank Dr. Mary Rezac and Dr. Peter Pfromm for their continued support, guidance, and patience throughout my Ph.D. program. They provided invaluable leadership and direction for me since I first arrived as an undergraduate REU student curious about research, but with little interest in attending graduate school. The conversations we've had and the examples they've set not only convinced me to apply to the KSU graduate program but have been great motivation for me to continue my own advancement. I was fortunate to have them both serve the role as my academic advisor.

I thank the current and past members of the Rezac/Pfromm research group who provided their experience and friendship to me: John Stanford, Michael Heidlage, Michael Wales, Yixiao Li, Lesley Schulte, and Matthew Young. I must also single out Matthew for all his assistance and the groundwork he laid to make my research possible. Thank you do Dr. Chris Sorensen for taking the time to serve as outside chair and his additional contributions.

Thank you to the rest of my committee. Dr. Bruce Law generously allowed access to his laboratory and provided guidance for research direction on several occasions. Dr. Gurpreet Singh provided a knowledgeable outside opinion and his interest in my work served as additional motivation.

Thank you to the Chemical Engineering Department staff for all their help: Danita Deters, Karen Strathman, Debi Wahl, Cynthia Brott, and Dave Threewit.

Special thanks are owed to my parents for their continuous support, and to my fiancé Celia for her love, patience, and especially her willingness to leave New England and move to Kansas with me as I pursued my Ph.D.

This material is based upon work supported by National Science Foundation Grant: From Crops to Commuting: Integrating the Social, Technological, and Agricultural Aspects of Renewable and Sustainable Biorefining (I-STAR); NSF Award No.: DGE-0903701 and the National Institute of Food and Agriculture, U.S. Department of Agriculture, under Agreement No. 2011-67009-20055.

Dedication

To Mom, Dad, Jeff, Jordan, and Celia for their love, support, and patience.

1 Introduction and Motivation

In the chemical industry, catalysts are used to increase the rate of chemical reactions that are thermodynamically favored but proceed at an uneconomical rate if not catalyzed. Catalysis is applied in 80% of synthetic chemical production. [1] In heterogeneous catalysis a solid catalyst is contacted with a gas or liquid phase that contains the reactants. Here, heterogeneous liquid phase catalysis is the focus, and in particular the hydrogenation of organic molecules in the liquid phase over metal catalysts such as palladium (Pd).

Pd is often chosen due to its viability as a catalyst for a variety of reaction applications including automobile catalytic converters, [2] petrochemical processing, [3] soybean oil hydrogenation, [4] pharmaceutical and fine chemical production, [5] and the conversion of biomass to chemicals. [6] In 2012, global Pd demand for catalytic converters and chemical production was 206,000 kg and 16,500 kg, respectively. [2]

For all catalytic hydrogenation processes, the interaction of hydrogen with the catalyst is the basis of the reaction scheme. Palladium is usually deposited on the external and internal surfaces of supporting porous particles such as carbon and pumice. [7, 8, 9] This means that reactants must diffuse through any boundary layers of stagnant fluid around the particles, and then often must diffuse in the pores of the particles to reach catalytic sites. Discussions below may refer to catalyst particles, and it should be understood that these particles usually are porous with catalytic metal deposited on external and internal surfaces. Heterogeneous catalytic hydrogenation is traditionally performed in a three-phase slurry reactor. [10] Hydrogenation occurs by the Horiuti–Polanyi Mechanism. [11] Catalyst particles are dispersed in a stirred liquid solution which is pressurized by hydrogen gas (Figure 1). Hydrogen is usually bubbled through the liquid where the catalyst particles are suspended. It then dissolves in the liquid, diffuses through boundary layers of the

particles, adsorbs to the catalyst surface, and reacts with incoming molecules. Products then diffuse away from the surface. The rate of heterogeneous catalysis is often restricted by mass-transfer limitations. The solubility of reactant gases, such as hydrogen, is relatively low in liquids, which causes a physical limitation on the amount of hydrogen that can reach active reaction sites. This can result in undesirable side reactions, lower product conversion rates, or the buildup of detrimental byproducts which can poison the surface. [10, 12] Hydrogenation reactions are also often performed at elevated temperatures (100-500 °C) to increase reaction rates, setting up a tradeoff between increasing reaction rate, and decreasing availability (solubility) of hydrogen in liquids. Hydrogen pressure in three-phase reactors ranges from 10 to 100 bar, demanding significantly more energy for compression than for reactions performed near atmospheric conditions. Scaling these reaction conditions to an industrial level incurs high capital and operating costs.

Due to the above limitations of heterogeneous liquid-phase hydrogenation, there is a motivation to develop other approaches to liquid-gas-solid contacting. Catalytic membrane reactors (CMRs [13]) are one innovative approach to catalyze gas phase reactions. However, one can also use membranes to separate liquid and gas phases while simultaneously providing selective delivery of reagents like hydrogen to catalyst sites. Membranes can generally be fabricated using metals, ceramics, and trapped liquids, but most membranes used commercially are derived from polymers. While typically utilized commercially for the separation of gas streams [14], these membranes can also be used to supply gas to a liquid reactant. [4, 15] Permeation of reactant gases through the membrane directly to the solid/liquid catalyst interface bypasses the hydrogen solubility limitations of slurry reactors, allowing for reactions to be carried out at lower temperatures and pressures. Singh et al. demonstrated the advantages of CMRs for improving

hydrogen availability by using them for the partial hydrogenation of soybean oil over Pd sputtered on the skin of a polymer membrane [4]. The increased availability of hydrogen can also enhance reaction kinetics and product selectivity, as well as prolong the life of the catalyst. Figure 2 shows a schematic of a CMR that uses an asymmetric polymeric membrane decorated with a metal catalyst for hydrogenation. Unlike the conventional three-phase reactor, as little as one atmosphere of hydrogen pressure suffices to drive the hydrogen transport to achieve full catalyst coverage.

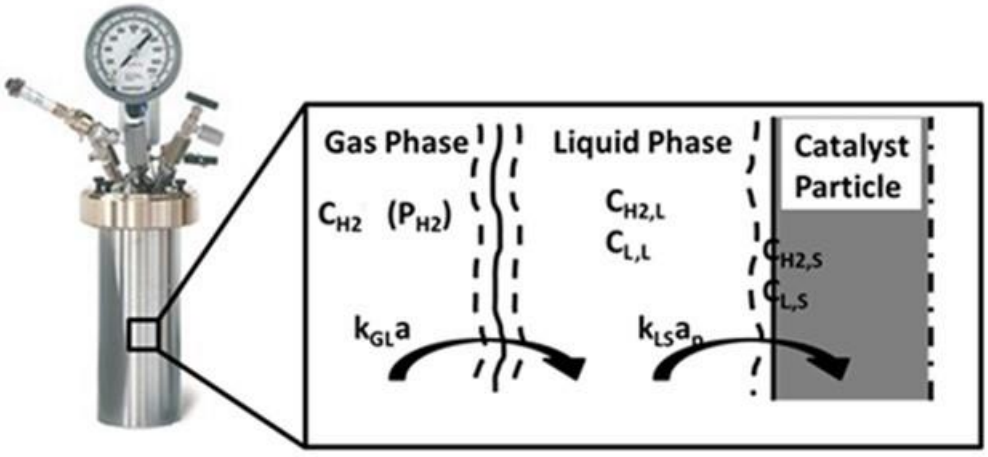

Figure 1. Conventional three-phase reactor system showing the process for hydrogen delivery to the catalyst surface. C_{H2} is the hydrogen concentration in the gas phase (analogous to pressure) $C_{H2,L}$ and $C_{L,L}$ are the hydrogen and liquid concentrations in the liquid phase, respectively. $C_{H2,S}$ and $C_{L,S}$ are their concentrations at the solid catalyst surface. k_{GL} and k_{LS} are the rate constants of transport at the respective gas-liquid and liquid-solid interfaces, while a and a_p are the interfacial areas.

The study of CMRs has typically focused on their performance based on variations in membrane properties, hydrogen availability, operating temperature, catalyst type, and catalyst deposition. However, fundamental questions about the interaction of hydrogen with the catalyst and the effects of catalyst morphology on these interactions are still of interest. Many techniques

have been developed for the study of catalytic interfaces [16], but are usually restricted by sample characterization and experimental conditions. Atomic force microscopy (AFM) is a surface characterization technique that is operated at room temperature and atmospheric pressure but can be extended to high pressure and temperature [17] [18]. By observing the magnitude and time dependence of the forces interacting between a sample and the fine tip of the AFM probe, topographical and material characterization data is gathered.

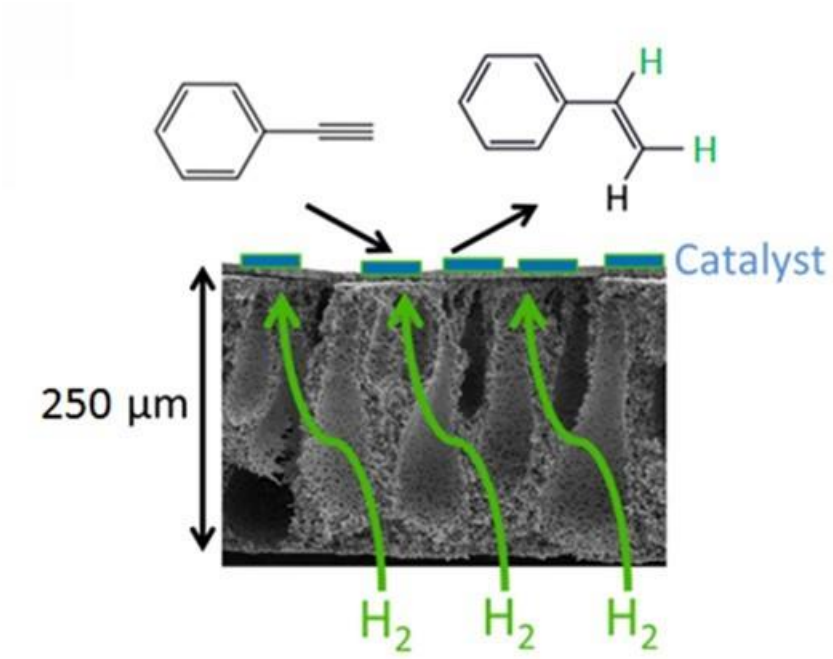

Figure 2. Operating principle of a catalytic membrane reactor. Hydrogen penetrates the porous support structure of the integral-asymmetric polymer membrane by convective transport, then dissolves in the non-porous thin top layer and diffuses through the non-porous layer to the catalyst. Hydrogenation of phenylacetylene to styrene is shown.

AFM [19] probes the surface of a sample with a microscale cantilever which approaches or contacts the surface using a fine tip and provides nanoscale resolution as it scans in a raster path along the x-y plane. In tapping mode, the probe is oscillated above the surface by a piezo crystal. The frequency of oscillation is the resonant frequency, or the frequency at which the probe is most responsive to changes in excitation [20]. The forces between the surface and the tip of the probe

can cause a delay in the oscillation of the cantilever relative to the piezo crystal's oscillation, which is observed and recorded as a quantifiable shift in phase. AFM has typically been used to observe surface topography in air, or soft matter under liquid in biology-related work, but recent work [21, 22] focused on the AFM phase angle data of a "hard" Pd surface under water. This phase data was represented as a time-dependent plot of the surface changes when exposed to hydrogen and nitrogen, as well as the hydrogenation of an oxygen monolayer from the Pd surface to form water. [23] The results showed for the first time that the subtle event of hydrogen appearing on the surface of palladium can be tracked with both spatial and time resolution by phase shifts of the AFM signal. The results agreed well with fundamental studies of hydrogen interaction with palladium near the gas/solid interface.

1.1 Research Objectives

- Verify by gas chromatography that the Pd-catalyzed hydrogenation of phenylacetylene (PhA) to styrene (St) and ethylbenzene (EB) takes place within a CMR at ambient conditions using a custom reactor setup that mimics the surface and events to be analyzed later by AFM.
- Use phase angle AFM to observe the changes in the catalyst surface over the course of the hydrogenation by analyzing phase shift data.
- Observe the changes in phase shift during an AFM scan when St is manually injected into an EB-immersed system, as well as the reverse case where EB is injected into St-immersed system.
- Link the observed phase shift trends to expected dynamic changes in surface chemistry.

2 Model reaction: Hydrogenation of Phenylacetylene

A model reaction must be selected to demonstrate that phase angle AFM can track catalytic hydrogenation on palladium in the liquid phase in real time, with hydrogen supplied by diffusion through the palladium layer at room temperature and atmospheric pressure to accommodate requirements of AFM instruments in the liquid phase. Hydrogenation of phenylacetylene is a very well characterized hydrogenation reaction that has been widely used to probe heterogeneous hydrogenation in the liquid phase. This reaction proceeds at room temperature and atmospheric pressure. [7, 24, 25, 26, 27]

The solvent-free catalytic hydrogenation of phenylacetylene (PhA) to styrene (St) can be performed over a Pd surface [28] and at ambient conditions. [28, 29, 30] The C-CH triple bond in the PhA structure is hydrogenated, converting it to a double bond $HC=CH_2$. As the reaction continues, the St is hydrogenated further to ethylbenzene (EB) as the double bond is broken to form a $H_2C\text{-}CH_3$ single bond. The reaction mechanism is shown schematically in Figure 3 and Figure 4.

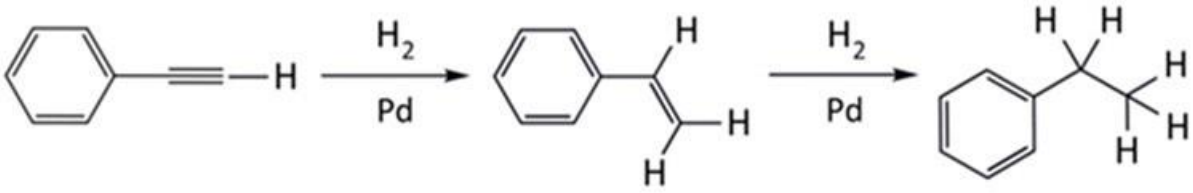

Figure 3. Sequential hydrogenation of phenylacetylene to styrene, and styrene to ethylbenzene, using a palladium catalyst deposited on a polymer membrane.

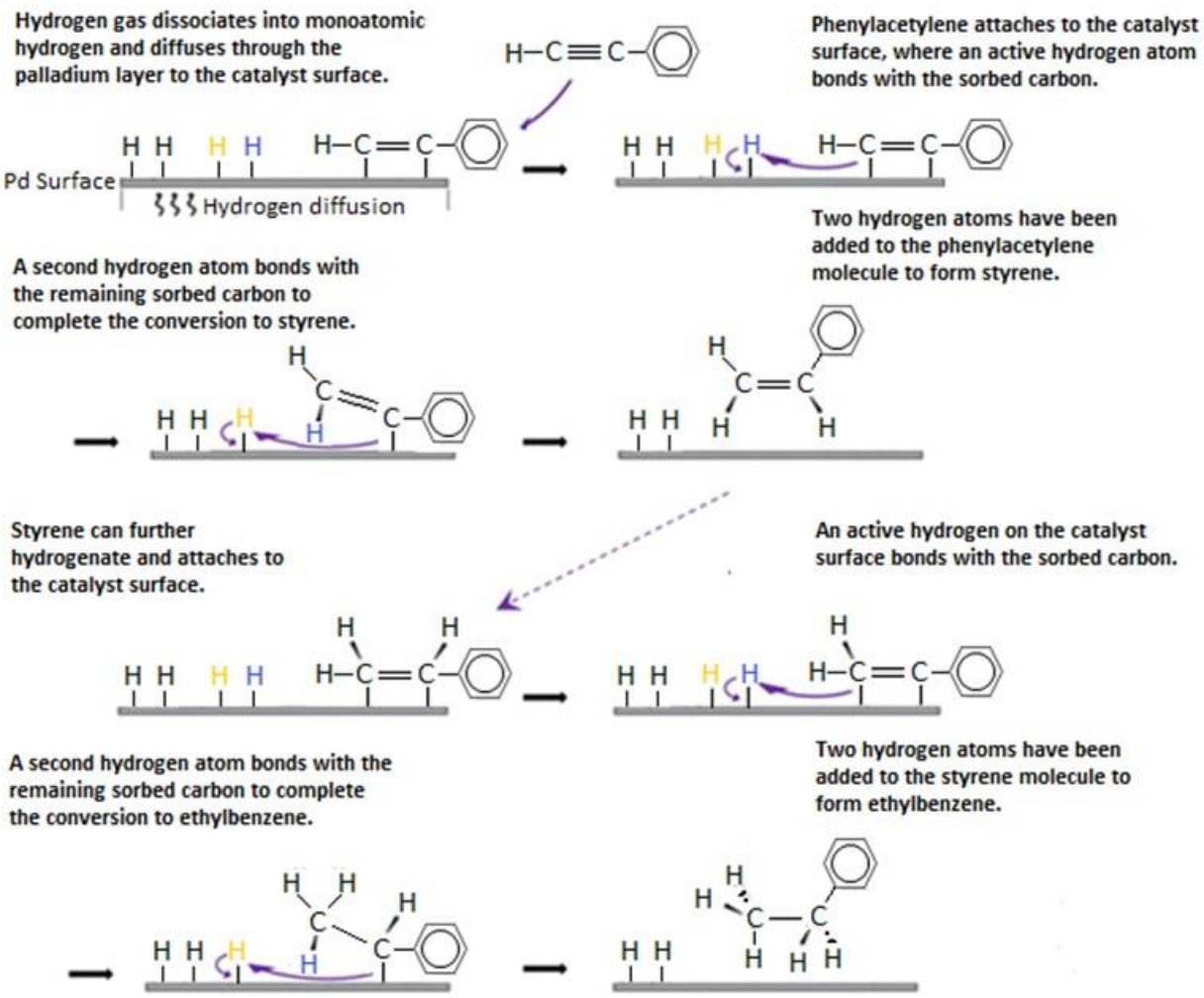

Figure 4. Reaction mechanism for the hydrogenation of phenylacetylene to styrene using a palladium-sputtered membrane [29, 31]. The reaction is stereospecific [32], always resulting in a syn-addition.

3 Experimental

3.1 Materials

The atomic force microscope is an Asylum Research MFP-3D instrument operated in AC mode using WaveMetrics Igor Pro 5.0.5.7 software. Olympus Corporation model BL-AC40TS nitride cantilever probes with rectangular silicon tips (≈ 9 ± 2 nm diameter) are used. Ethanol (Sigma-Aldrich, ACS reagent, ≥99.5 wt%), toluene, and chloroform (both Fisher Scientific, Certified ACS, 99.9 wt% assay) are used for rinsing the probes. Phenylacetylene (Fisher Scientific, 98 wt% Pure) is used as a reacting liquid and scanning medium. Styrene (Fisher Scientific, 99.5 wt%) and ethylbenzene (Fisher Scientific 99.8 wt%, anhydrous) are used to prepare GC standards. Styrene and ethylbenzene were also used as liquid phase during AFM scanning.

Hydrogen and nitrogen (Ultra High Purity, 99.999 vol% purity) was acquired from Matheson Tri-Gas (Manhattan, KS). Gas flow was supplied via a custom manifold of Swagelok 316 stainless steel valves and tubing (Kansas Valve and Fitting, Kansas City, KS). Palladium-sputtered or blank film samples were attached to a custom-made aluminum sample holder using LocTite Quick Set epoxy.

Teflon samples were cut from a 60 x 12 in. roll of nonporous, 127 μm thick PTFE (ePlastics, San Diego, CA). A 99.95 wt% Pd sputter target (Ted Pella, Redding, CA) using a DESK II magnetron sputter coater (Denton Vacuum, Moorestown, NJ was used for sputter coating.

Gas chromatography (GC) was used to analyze reaction samples. A flame ionization detector (FID) provided component identification using a GS-GASPRO 113-4332 column (30m length, 0.32mm ID, Agilent Technologies, Santa Clara, CA) with the settings listed in Table 1.

Table 1. GC system settings

Detector Temp	220 °C
Inlet Temp	220 °C
Oven Temp	200 °C
Carrier Gas	Argon
Inlet Pressure	37.75 psig
Column Flow	6.0 mL/min
Split Ratio	30:1
H_2 Flow	50.0 mL/min
Air Flow	450 mL/min
Makeup Flow	32.1 mL/min

3.2 Methods

3.2.1 Preparing a Pd-sputtered PTFE sample

Teflon samples were cut into 4.1 cm diameter circles. Select samples were sputter-coated with palladium for 45 s with a current of 45 mA under 100 mTorr argon. The 45 second sputter time was divided into three separate treatments of 15 s each for a total estimated metal layer thickness of 12 nm [33].

3.2.2 Reaction cell for GC confirmation of reaction

The presence of the expected chemical reaction was demonstrated by hydrogenation of phenylacetylene to ethylbenzene in a 4.7 cm diameter test cell with 14.5 cm^2 of active area. The structure of the palladium/PTFE composite was identical to the structure used later in AFM experiments. The Pd-PTFE composite was prepared according to the method described in chapter 3.2.1

3.2.3 GC Analysis

To verify that the desired reaction was taking place, a similar reactor system to the one used for the AFM was built to be analyzed by Gas chromatography (GC) (Figure 5). This reactor was

also covered to minimize evaporation and extend operating time. Hydrogen was supplied to the underside of the enclosed membrane test cell at the same 2.0 L(NTP)/min flow rate used during AFM experiments. After 30 minutes, liquid phenylacetylene was added to the Pd-coated side of the sample. A 0.5 µL volume of the reactant was analyzed by GC/FID to verify the lack of an ethylbenzene product peak prior to the reaction. The reaction was run for 8 hours with 0.5 µL samples taken for GC analysis every 2 hours, and then additional samples were taken at 24, 26, and 28-hours. UniChrom™ software was used to process the GC data.

The reaction of PhA to St and EB (Figure 3) was tracked by sampling the liquid in contact with the palladium where hydrogen emanates from the palladium layer. The sample volume was 0.5 µL, or about 0.026% of the total liquid volume in the test cell. The liquid was not stirred during reaction but was shaken gently prior to each sample.

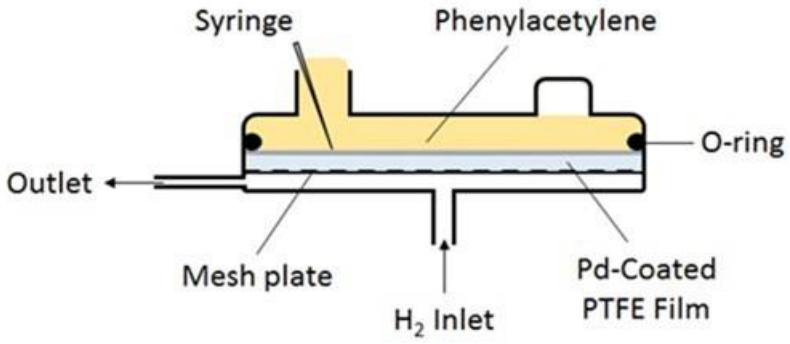

Figure 5. Schematic of the 1.9 mL capacity test cell used for proof of reaction. H_2 gas is supplied underneath the sample, passing through the metal mesh support plate to the PTFE side of the sample. H_2 diffuses through the PTFE layer to the Pd coating, where it dissociates to monoatomic hydrogen and diffuses through to the surface to react with the liquid PhA 0.5 µL samples for GC were taken via syringe from the open port. The port was covered between samples to minimize evaporation.

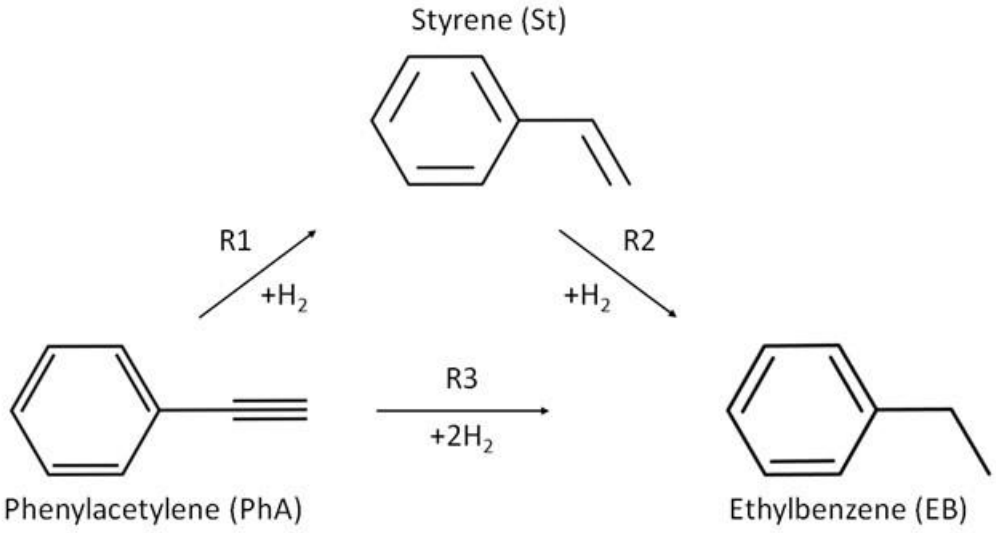

Figure 6. Phenylacetylene hydrogenation reaction pathways.

3.3 AFM methods

3.3.1 Installing the AFM probe

The AFM cantilever probe was placed into its holder and rinsed successively with ethanol, toluene, and chloroform. The probe was then dried with N_2 gas and installed in the AFM head. The sample to be scanned was rinsed with ethanol, dried with N_2 gas, and positioned on top of the AFM base such that the aperture in the sample holder would be aligned as much as possible with the tip of the cantilever probe during scanning. The AFM head was then placed onto the base, and the laser position adjusted as necessary to achieve a relative maximum SUM signal over the tip of the probe.

For liquid scans, a small volume of liquid (phenylacetylene, styrene, or ethylbenzene) was added into the sample holder on top of the sample. 1.8-2.0 mL of liquid was used for scans where no further liquid was to be injected. For scans where injections were to be made, an initial volume of 1.5 mL was added to cover the probe, but not flood the cantilever holder upon further addition

of liquid. Visual confirmation of the probe being covered was achieved by observing the SUM signal dropping due to deflection of the laser in the liquid. The position of the AFM laser was then adjusted until a new relative maximum SUM signal was achieved in the liquid medium. The cantilever deflection was adjusted to zero using the PD thumbwheel, and the system was then left for at least 30 minutes to allow it to reach equilibrium. This was confirmed by the deflection signal remaining constant for at least 60 seconds.

3.3.2 Cantilever tuning procedure

Once the deflection signal stabilized, it was readjusted to zero and the cantilever was tuned. A thermal tune was performed for 100 counts at the normal rate, and the drive frequency was set to the dominant peak. This peak typically appeared at 46, 51, or 61 kHz. The drive amplitude was set to a value such that the one tune amplitude of the dominant peak was approximately 1.0 V. The set point was raised to 90% of the drive amplitude, and the probe was engaged. The AFM head was lowered slowly until there was an audible tone, indicating the probe had nearly contacted the sample surface.

It was observed that after performing a single tune in a liquid medium, there was still significant noise during scans and difficulty achieving trace/retrace overlap. For this reason, a second tune was implemented for liquid scans. After completing the first tuning sequence, the tip was disengaged, and deflection was readjusted to zero if necessary. The thermal tune was performed again for 100 counts at the default ("normal" by the software) rate of approximately 3 counts per second, and the drive frequency to set to the highest peak, typically occurring at ~25 kHz, 45 kHz, 51 kHz, or 62 kHz, though the most stable phase trace data was observed at 25 kHz and is described later. It is noteworthy that the peak response was generally much stronger during the second tuning sequence, characterized by the same tune amp voltage being achieved with

smaller drive amplitudes. Drive amplitude was then adjusted such that the chosen frequency peak reached an apparent maximum, and further increase would result only in lowering the Q value or flattening of the frequency peaks. Set point was adjusted to 90% of the drive amplitude. The tip was then engaged with the surface (which requires little motion due to having performed the tune just above engagement) and lowered until Z voltage ~70V. Set point was lowered until the deflection and amplitude signals were relatively constant, and the phase value fluctuated by only a few degrees. The scan was then started, and set point was adjusted as necessary to achieve overlap in the height trace/retrace plots. As such, any significant noise in the data within the first few minutes of scanning can be attributed to this set point adjustment unless stated otherwise.

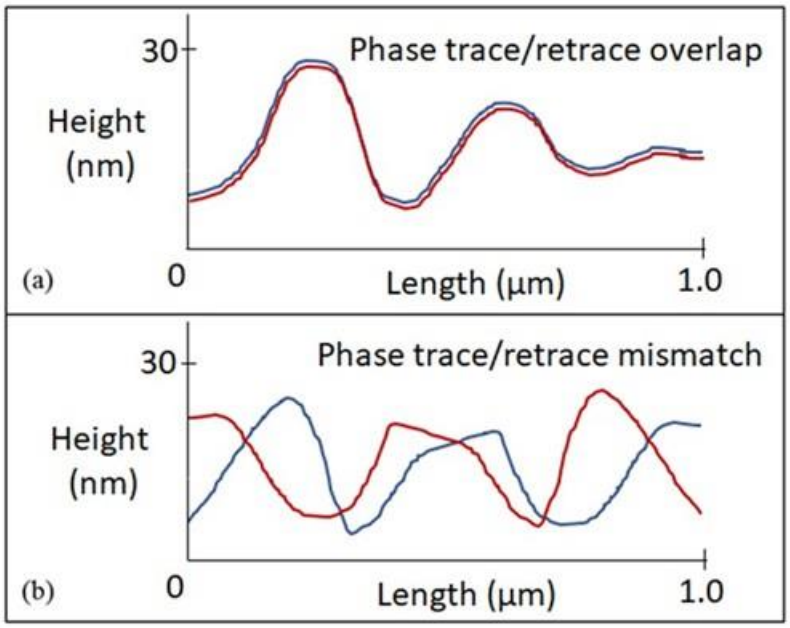

Figure 7. Example of phase trace/retrace plots observed during scanning. Box (a) represents an ideal trace/retrace overlap used during scanning at the respective set point. Box (b) represents a phase trace/retrace plot that is mismatched, and so the set point must continue to be adjusted until an overlap is reached.

3.3.3 Determining optimum drive frequency

After the second tuning process, new peaks in the drive frequency plot were observed. Specifically, a peak at 25-26 kHz seemed to consistently achieve the most stable scans when compared to those performed at higher frequency. This was true even if it was not the dominant peak, defined here as the frequency at which the highest tune amplitude voltage peak appeared for a given drive amplitude. For consistency, drive amplitude was adjusted such that the relatively smaller 25-26 kHz peak still reached a one tune amplitude of ~1.0 V. Scans were performed in this range whenever possible as indicated in the discussion of results, otherwise the dominant peak was used.

3.3.4 Performing an AFM Scan in Liquid

For scans with nitrogen flowing initially, gas flow was started just prior to tuning. For scans with an initial flow of hydrogen, H_2 flow through the sample holder was applied for 30 minutes to establish hydrogen diffusion through the Pd layer to the surface prior to reactant addition. Gas flow rate was ~2.0 L(NTP)/min. The respective immersion liquid was added to the sample surface, covering the cantilever. Tuning was performed in accordance with chapter 3.3.2. Gas switching was performed as noted to observe any noise caused by manipulation of valves during scanning, as well as any potential trends in phase data caused by the change in the supplied gas. Liquid injections were performed as noted with varying volumes and were always supplied just under the outer edge of the AFM cantilever holder, 1 cm from the scan area.

3.3.5 Data Exclusion Guidelines

While there are methods for reducing the impact of impurities and noise, not all scans provide useful data. Some guidelines have been developed for determining when to disregard a scan: (localized areas of noise or erratic phase data may not disqualify an entire scan)

- Sloping baseline: In the 2D line averaging plot, because the surface is assumed to be uniform, the phase trace average during periods of relative inactivity should also be somewhat constant. If the phase trace average continuously increased or decreased over the course of a scan where there are no system changes, the data was not used.
- Erratic phase trace: For scans where system parameters are kept constant, the data was not used if phase trace varied by more than 10 degrees.
- Noisy amplitude plot: The AFM was operated in constant amplitude mode, where the deflection of the cantilever is kept constant over the course of the scan. If the 3D amplitude plot was observed to be noisy, the scan data was not used.
- Asymmetry in sequential scans: For sequential scans where the liquid medium was unchanged, the scan data was not used if the topography images were not reasonably symmetrical.
- Phase trace changes in sign at 180°: Phase trace data was not used if it was operated on the border of +180°/-180° due to inability to accurately average the individual lines of data.

4 Confirming the Hydrogenation of Phenylacetylene in a Custom Catalytic Membrane Reactor at Ambient Conditions

The model reaction of the hydrogenation of phenylacetylene (Figure 3) was confirmed to proceed at the same conditions and over the same palladium (Pd) coated PTFE film as used later in the AFM scanning experiments. First, a maximum reaction rate was established by estimating the hydrogen flux that is supplied to the catalyst surface by permeation. Hydrogen permeation through the PTFE and Pd layers of the sample depends on each layer's thickness and intrinsic permeability to hydrogen, which is related to diffusivity and solubility by the following equation:

$$P = D \cdot S \qquad \text{Equation 1}$$

where P is the permeability $\left(\frac{\text{mol H}_2}{\text{cm·s·MPa}}\right)$, D is the diffusion coefficient $\left(\frac{cm^2}{\text{s}}\right)$, and S is the solubility $\left(\frac{\text{mol H}_2}{\text{cm}^3\text{·MPa}}\right)$. These values are tabulated below for hydrogen gas in Pd and PTFE at room temperature. Permeability is calculated from literature values.

Table 2. Diffusion coefficient, solubility, and permeability of hydrogen in PTFE and Pd at 25°C for mass transfer calculations.

Material	**D (cm^2/s)**	**S (mol H_2/cm^3·MPa)**	**P (mol H_2/cm·s·MPa)**
PTFE	$1.47 \cdot 10^{-7}$ [34]	$2.20 \cdot 10^{-4}$ [34]	$3.23 \cdot 10^{-11}$
Palladium	$2.8 \pm 0.2 \cdot 10^{-7}$ [35, 36]	$4.03 \cdot 10^{-3}$ * [37]	$1.13 \cdot 10^{-9}$

* Performed at 27°C. Units converted from [cm^3(STP)/(cm^3 cmHg)]

The thickness of the palladium layer was determined to be 12 nm based on the sputtering process parameters [38]. Since the permeability of H_2 gas is two orders of magnitude lower in PTFE than Pd, and the 127 µm PTFE layer is four orders of magnitude thicker than the Pd layer, the sample can be approximated regarding mass transfer as a single layer of PTFE. Fick's First

Law of Diffusion allows a theoretical hydrogen flux to be calculated using permeability, material thickness, and the hydrogen pressure difference across the sample:

$$j = -\frac{P(p_2 - p_1)}{\delta} \qquad \text{Equation 2}$$

where j is the specific hydrogen flux (mol $H_2/cm^2 \cdot s$), δ is the sample thickness (cm), p_1 is the outlet pressure (MPa), and p_2 is the hydrogen pressure (MPa) at the sample surface, which is assumed to be negligible since hydrogen is consumed during reaction.

The molar flow rate of hydrogen through the sample is determined by:

$$J = j \cdot A \qquad \text{Equation 3}$$

where J is the molar flow rate $\left(\frac{\text{mol } H_2}{s}\right)$ and A is the area of the sample (cm^2). Since stoichiometry requires one H_2 molecule for each bond broken during hydrogenation, this H_2 flow rate is also a theoretical maximum production rate for the hydrogenation of phenylacetylene to styrene, or styrene to ethylbenzene.

Based on the above calculations, the maximum reaction rate based on hydrogen diffusion for a 13.38 cm^2 sample is about $1.75 \cdot 10^{-9}$ mol/s when reaction experiments are performed in the reaction test cell. This is compared in a later section to a theoretical maximum reaction rate based on known data. The difference between the diffusion and kinetics-based reaction rates will give an indication whether the system may be limited by hydrogen diffusion.

4.1 Gas chromatographic analysis

As expected, the ethylbenzene (product) peak was observed and grew over the course of the reaction, shown in Figure 10 and Figure 11. Due to the relative size of the phenylacetylene peak compared to styrene, and the small difference in boiling point and chemical composition, the styrene peak is lost in the PhA peak.

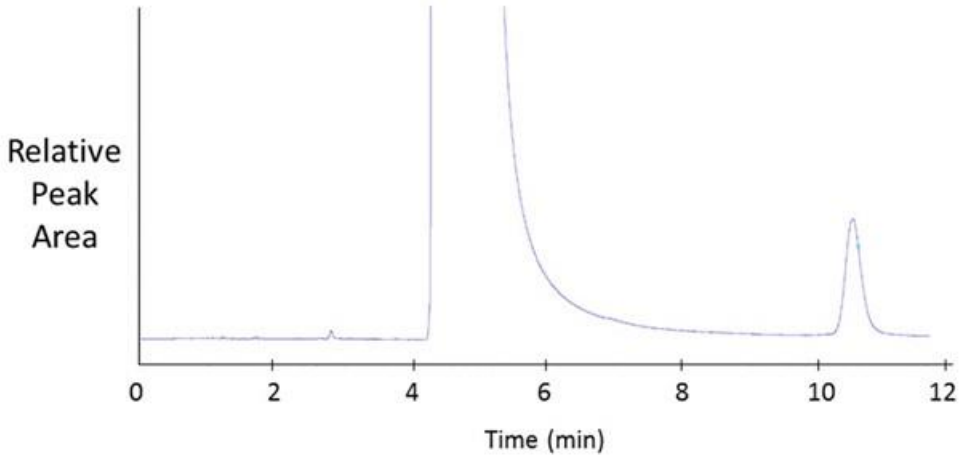

Figure 8. Chromatogram of 98% pure (as received) phenylacetylene. The large PhA peak begins at approximately 4.2 minutes. All smaller peaks likely correspond with impurities which appear in all reaction samples and are omitted from analysis.

GC data was analyzed using UniChrom™, an automated chromatographic data system, to obtain chemical peaks and integrated peak area. At low conversion rates (explained in greater detail later), the phenylacetylene concentration can be viewed as a constant. Under this assumption, the PhA peak area for each successive sample was normalized against the PhA peak area of the first sample. This ratio of peak areas provided a correction factor for the EB peak area to observe how EB content changed over the duration of the reaction.

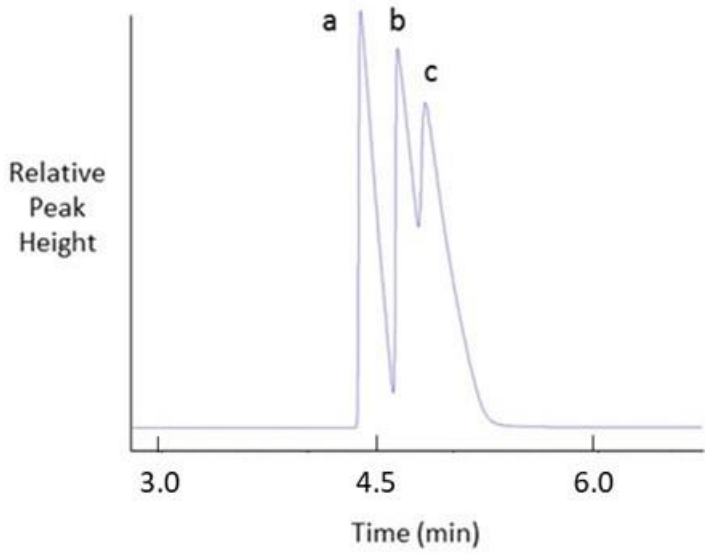

Figure 9. UniChrom™ chromatogram of an approximately 1:1:1 (a) ethylbenzene, (b) phenylacetylene, and (c) styrene mixture. The close retention times of phenylacetylene and styrene, exhibited by the split peak, make it difficult to identify styrene within a mixture that has a much higher phenylacetylene concentration.

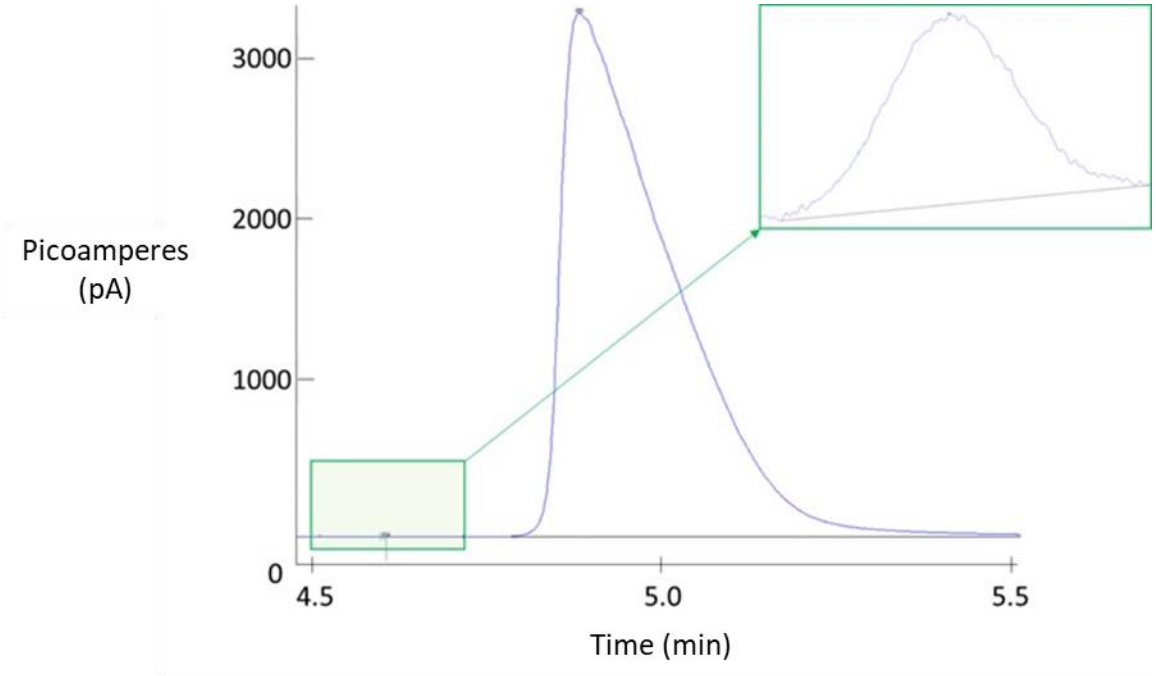

Figure 10. UniChrom™ chromatogram of the reaction test cell liquid after 24 hours of reaction. Ethylbenzene can be seen in the highlighted region. Styrene is subsumed underneath the large phenylacetylene peak.

To create a calibration curve for determining EB product content in the reaction sample, 0.5 μL of EB was diluted with PhA and analyzed with GC using the same settings outlined in the Experimental section. The volume of PhA and EB, and the mol% of EB for the calibration samples are listed below in Table 2. Peaks obtained for impurities in the phenylacetylene were omitted. Molar content was calculated from the following equation:

$$n_i = \frac{V_i \rho_i}{M_i} \qquad \text{Equation 4}$$

where n_i is the number of moles of PhA or EB, V_i is the volume added to solution (mL), ρ_i is density (g/mL), and M_i is molar mass (g/mol). The EB content (mol %) is then determined by dividing the molar content of EB by the total number of moles of EB and PhA and multiplying by 100%:

$$X_{EB} = \left(\frac{n_{EB}}{n_{EB}+n_{PhA}}\right) 100\% \qquad \text{Equation 5}$$

where X_{EB} is the mole percent of ethylbenzene.

Table 3. Chemical properties of phenylacetylene and ethylbenzene.

	Density at 25°C (g/mL)	Molar Mass (g/mol)
Phenylacetylene	0.930 [39]	102.13
Ethylbenzene	0.863 [40]	106.17

Table 4. Content of calibration samples used in the dilution of 0.5μL ethylbenzene.

	Volume PhA (mL)	Volume EB (μL)	Mol % EB
Sample 1	0.5 ± 0.05	0.5 ± 0.1	$9.0 \cdot 10^{-4}$
Sample 2	5.0 ± 0.2	0.5 ± 0.1	$9.0 \cdot 10^{-5}$
Sample 3	20.0 ± 0.2	0.5 ± 0.1	$2.2 \cdot 10^{-5}$

The phenylacetylene peaks were normalized to better observe the change in ethylbenzene concentration between samples. Since the reaction is performed at very low conversion, PhA concentration can be assumed to remain constant with respect to the amount of product. This means that for samples of the same volume, the area of the PhA peak should also remain constant. Samples were taken manually, introducing some human error to the volume of each sample. If $A_{PhA,0}$ is the area of the PhA peak $(\mathrm{mpA \cdot min})$ at the start of the reaction, then a correction factor (CF_t) for the PhA peak in subsequent samples can be found by the equation:

$$\mathrm{CF_t} = \frac{\mathrm{A_{PhA,0}}}{\mathrm{A_{PhA,t}}} \qquad \text{Equation 6}$$

where $A_{PhA,t}$ is the area of the PhA peak at time t (hr). This correction factor can then be used to normalize the EB peak area for the sample taken at time t:

$$\mathrm{A^*_{EB,t}} = \mathrm{A_{EB,t}} \cdot \mathrm{CF_t} \qquad \text{Equation 7}$$

where $A_{EB,t}$ is the absolute EB peak area, and $A^*_{EB,t}$ is the corrected value. The curve then better reflects reaction progress:

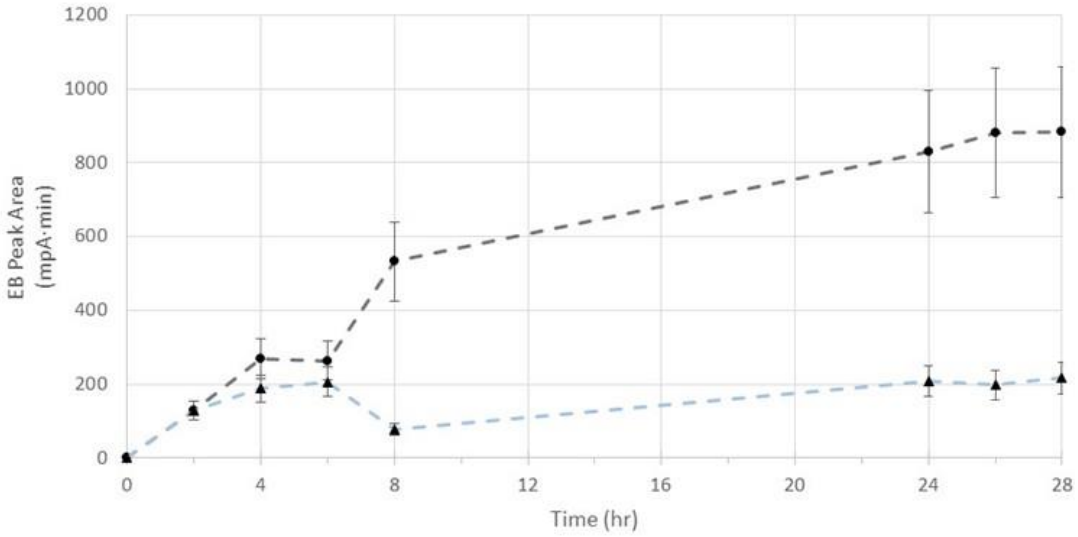

Figure 11. Corrected (●) and absolute (▲) ethylbenzene peak area as a function of time. Error is due to 0.5 μL sample volume using a syringe with 0.1 μL graduations.

The molar content (mol%) of ethylbenzene was plotted as a function of corrected peak area to observe their relationship. The plot is shown below in Figure 12.

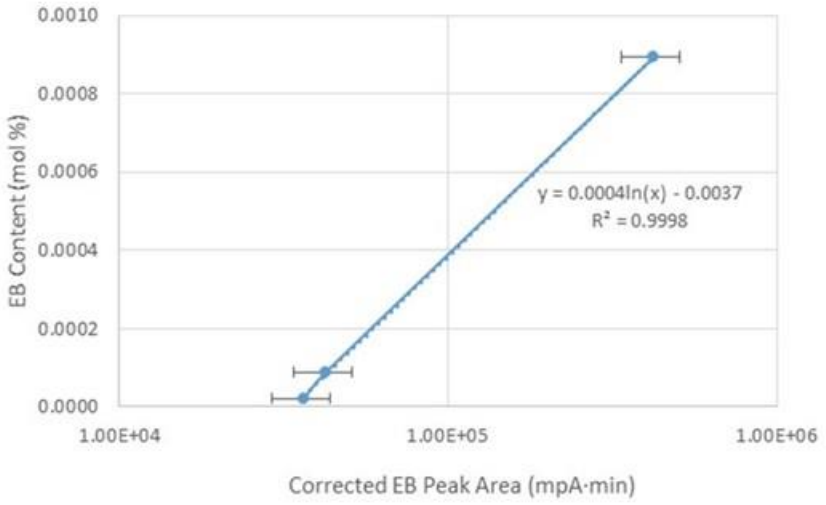

Figure 12. Semi-logarithmic plot of EB concentration as a function of corrected peak area. Error in the x-direction is due to the GC syringe. Error in the y-direction is minimal and contained within the data points.

The dependence of EB content on peak area in Figure 12 appears to be logarithmic, but the sample size is too limited to extrapolate the plot to lower concentrations. While this coincides with the order of magnitude of dilution, further data needs to be gathered to determine the precise relationship, especially at concentrations closer to those expected during the reaction. It is expected that a more exhaustive calibration curve would exhibit linear behavior. [41]

It has been shown that the hydrogenation of phenylacetylene and styrene is initially zero-order in both species. [27] At 60% conversion the kinetics change to first-order due to competitive adsorption between the species to the catalyst surface. If the reaction is hydrogen starved, this competitive sorption may be able to take place at a much lower conversion. This is possibly the cause for the non-linearity in the production rate of ethylbenzene seen here.

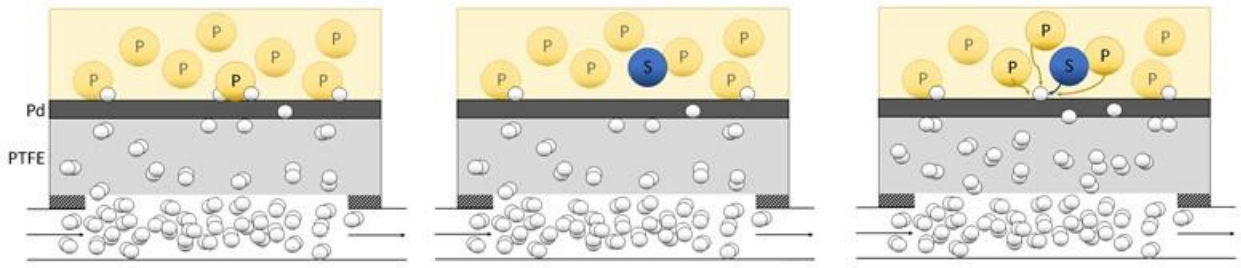

Figure 13. Schematic representation of the liquid-solid interface during phenylacetylene hydrogenation to styrene.

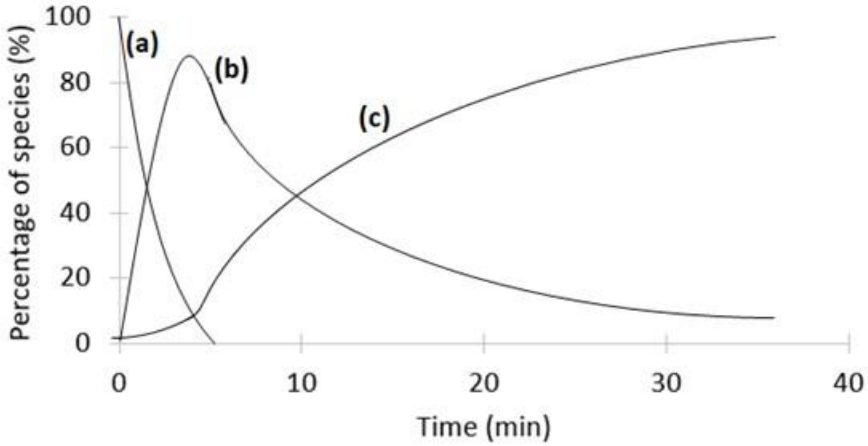

Figure 14. Percentage of reactant and products as a function of time for the hydrogenation of (a) phenylacetylene to (b) styrene and (c) ethylbenzene (modified after Duca et al. [9]). At extremely low conversion, the production of both St and EB can be approximated as linear functions of time, with the rate of St being much faster than EB due to the difference in slopes.

The hydrogenation of phenylacetylene has been verified using the designed CMR at ambient conditions by GC. The catalytic membranes were identical to the Pd-sputtered films used later for AFM experiments to track the same reactions. Variability between samples, reflected in the data, requires a normalization to be performed to better interpret the reaction progress. This normalization is outlined in the next section.

4.2 Estimate of the hydrogen demand for hydrogenation of phenylacetylene over sputtered palladium

Three-phase hydrogenation reactions are typically performed using catalyst particles to maximize the catalyst surface area, which is analogous to the number of active sites. Instead of the catalyst being deposited on support particles, the catalyst in this research is over a sputter-coated, flat plane of palladium. To estimate the required hydrogen availability and conversion rate of the system, certain modifications must be made to adjust for this difference in catalyst morphology compared to most published work.

Turnover frequency (TOF) is defined as the number of moles of a specific product formed for each mole of catalyst per second. This helps describe the rate of conversion from reactants to products in a 3-phase slurry reactor for a specific loading of catalyst particles. In a catalytic membrane reactor (CMR) [4], the reaction takes place exclusively at the planar surface due to the impermeability of the metal catalyst layer to the reacting liquid. By converting TOF from moles/mol catalyst per second to moles/cm^2 catalyst per second (TOF'), the value becomes useful in describing the membrane surface.

When prepared in solution, the number of moles of catalyst can be determined from the concentration and volume of the catalyst solution. For a palladium catalyst, the total moles of palladium is:

$$n_{Pd} = C_{Pd}V \qquad \text{Equation 8}$$

where n_{Pd} is the amount of palladium in moles, C_{Pd} is the palladium concentration in mol/L, and V is the volume of solution in liters.

The mass of palladium catalyst in solution is determined simply by multiplying the number of moles by the molecular weight:

$$m_{Pd} = n_{Pd} M_{Pd} \quad \text{Equation 9}$$

where m_{Pd} is the total mass of palladium catalyst particles in g and M_{Pd} is the molecular weight of palladium in g/mol. This value will be used to determine the effective surface area of palladium for the catalyst particles.

The available palladium surface area is determined by using the palladium mass and specific surface area. The palladium particles used for reference rest on a pumice support, so the areas of contact between the two materials would not be available for reaction. This lost surface area is not accounted for in calculations, but its impact will be explained at the end of the section. The palladium surface area is given by:

$$A_{Pd} = m_{Pd} A_{s,Pd} \quad \text{Equation 10}$$

where A_{Pd} is total palladium surface area in cm^2 and $A_{s,Pd}$ is the specific surface area of palladium particles in cm^2/g. Palladium particle size and specific surface area were reported by Fagherazzi et al. [8]

Turnover frequency is the number of moles of a product formed for each mole of palladium per second. With the number of moles of palladium and the available palladium surface area now calculated, TOF can be converted to a value that represents the number of moles of product formed per unit area of catalyst per second. This value will be referred to as the adjusted turnover frequency (TOF'), given by:

$$TOF'_i = TOF_i \left(\frac{n_{Pd}}{A_{Pd}}\right) \quad \text{Equation 11}$$

where TOF'_i is the number of moles of product i formed per cm^2 palladium per second. This value is calculated for each reaction product (PhA to St, St to EB, PhA directly to EB) and combined to determine the total number of moles of product formed per unit area of catalyst per second.

For the planar catalyst surface in a CMR, TOF' can be multiplied by the area of the catalyst surface to determine the theoretical maximum amount of product generated per second, assuming adequate hydrogen availability. This value can also be viewed as a theoretical minimum required H_2 availability to prevent the reaction from being limited by hydrogen transport.

Table 5. Catalyst properties based on literature values and calculations.

Pd particle radius (cm)	$1.4 \cdot 10^{-7}$ [7, 8]
$A_{s,Pd}$ (cm^2/g)	278 [8]
M_{Pd} (g/mol)	106.42
ρ_{Pd} (g/cm^3)	11.9
C (mmol Pd/L)	0.17 [7]
V (mL)	15 [7]
n_{Pd} (mol)	$2.55 \cdot 10^{-6}$
A_{Pd} (cm^2)	754.41

Table 6. Turnover frequency for the hydrogenation of phenylacetylene from literature, and the adjusted turnover frequency after converting from moles catalyst to area of catalyst. Multiplying by area yields theoretical minimum required H_2.

Reaction	TOF (mol/mol Pd·s) [9]	TOF' (mol/cm^2 Pd·s)	TOF' Total (mol/cm^2 Pd·s)	CMR Surface Area (cm^2)	H_2 Required (mol/s)
PhA → St	5.5	$1.9 \cdot 10^{-8}$	$3.1 \cdot 10^{-8}$	14.5	$4.6 \cdot 10^{-7}$
PhA → EB	0.2	$6.8 \cdot 10^{-10}$			
St → EB	3.6	$1.2 \cdot 10^{-8}$			

The adjusted turnover frequency can be interpreted as a required molar diffusion rate of H_2 necessary to ensure the reaction is not hydrogen starved. One molecule of H_2 is required to perform one reaction of PhA → St. This is also true for St → EB, so these TOF' terms can be added together. Since PhA → EB is a 2-step hydrogenation, this TOF' value is multiplied by 2. By

adding these terms together, the final value (TOF' Total) is the total amount of hydrogen required per unit area per second, assuming all H_2 supplied to the reaction surface is used for hydrogenation. By multiplying by the area of the sample (14.5 cm^2), the theoretical required H_2 molar flow rate is $4.6 \cdot 10^{-7}$ mol/s. The calculated H_2 diffusion rate (from section 4.1) is $3.7 \cdot 10^{-9}$ mol/s, which is over two orders of magnitude lower than the required flow rate. It can then be assumed that the hydrogenation taking place in this reactor system is hydrogen starved. For scans where styrene is used as the reaction medium instead of phenylacetylene, half of the hydrogen demand is removed. This only reduces the required H_2 by a factor of two ($2.3 \cdot 10^{-7}$ mol/s), and so the reaction is still hydrogen starved by almost two orders of magnitude.

In the pumice-supported palladium particle system, the areas where the metal contacts the support are not available for reaction due to inaccessibility of the liquid medium. These shielded areas result in a direct reduction in the available total palladium surface area. Were this to be taken into effect, the total palladium surface area in Equation 10, A_{Pd}, would *decrease*. However, since the amount of product generated remains the same, this would result in an *increase* in the adjusted turnover frequency calculated in Equation 11 due to it being inversely proportional to total surface area. Qualitatively, if less area is required for a given amount of palladium in a catalyst particle system to generate *n* moles of product, more surface area is required in the respective CMR. Since the CMR is already determined to be hydrogen starved, adjusting for lost surface area only pushes the system further in that direction.

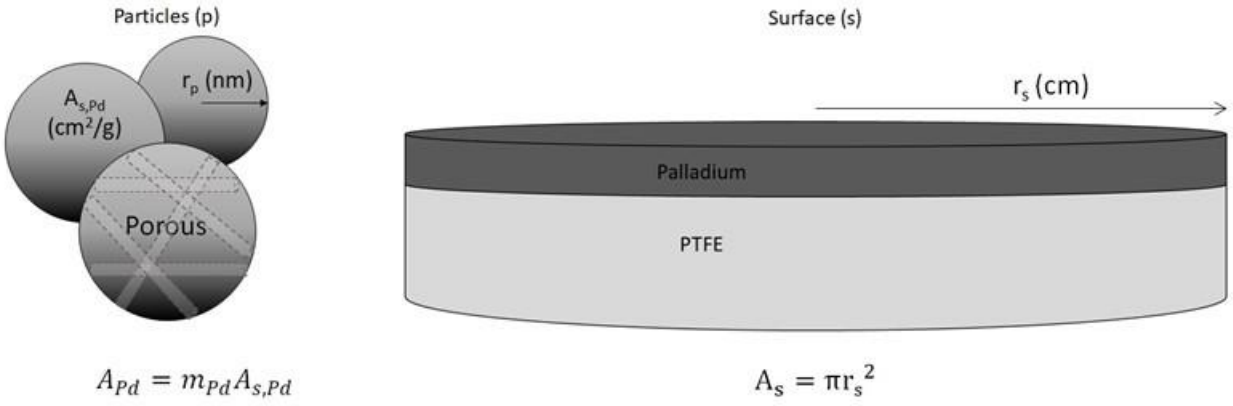

Figure 15. Comparing the available surface area of dispersed catalyst particles to a flat plane CMR surface. The area of the particles depends on the amount of loaded palladium and the average specific surface area of the particles. The area of the flat plane is determined simply by the circular area of the surface layer.

4.3 Conclusions from the Reaction Test Cell and Gas Chromatography

It has been shown using a catalytic membrane reactor that the hydrogenation of phenylacetylene and styrene to ethylbenzene is possible using a planar palladium catalyst similar to the one to be observed by AFM. This reaction is hydrogen starved and proceeds on a time scale not advantageous for continuous AFM observation, and so additional measures must be taken to observe real-time reaction conditions. The next chapter will discuss injecting ethylbenzene into a styrene covering the Pd surface mid-scan to observe surface-tip interaction changes as the reaction product appears at the surface. The reverse case was also observed, where reactive styrene was injected into an ethylbenzene-immersed scan.

5 Hydrogenation Visualization in AFM

The following table provides a generalized summary of the experiments performed under AFM observation and their respective purposes. Each experiment is explained in further detail below.

Table 7. Summary of experiments.

Surface	Gas/Sequence*	Immersion Liquid	Injection	Purpose	Chapter
Teflon	None	Phenylacetylene	None	Verify phase data coherence in model reaction liquid	5.2
Teflon	None	Phenylacetylene	None	Observe how equilibration time affects phase noise	5.2
Teflon	N_2-H_2	Phenylacetylene	None	Observe how gas flow affects phase noise	5.3.2
Palladium	N_2-H_2	Styrene	None	Verify H_2O formation visible in styrene	5.4
Palladium	H_2	Styrene	EB	Observe if injection-simulated reaction is visible in phase data	5.4
Palladium	N_2-H_2	Ethylbenzene	None	Verify H_2O formation visible in ethylbenzene	5.5
Palladium	H_2	Ethylbenzene	EB	Observe no change in surface chemistry = no change in phase trace	5.5
Palladium	H_2	Ethylbenzene	St	Observe if/how change in surface chemistry affects phase trace data	5.5

*Switching the supplied gas also tested if valve manipulation affects phase noise.

5.1 Sample system and 3D data analysis

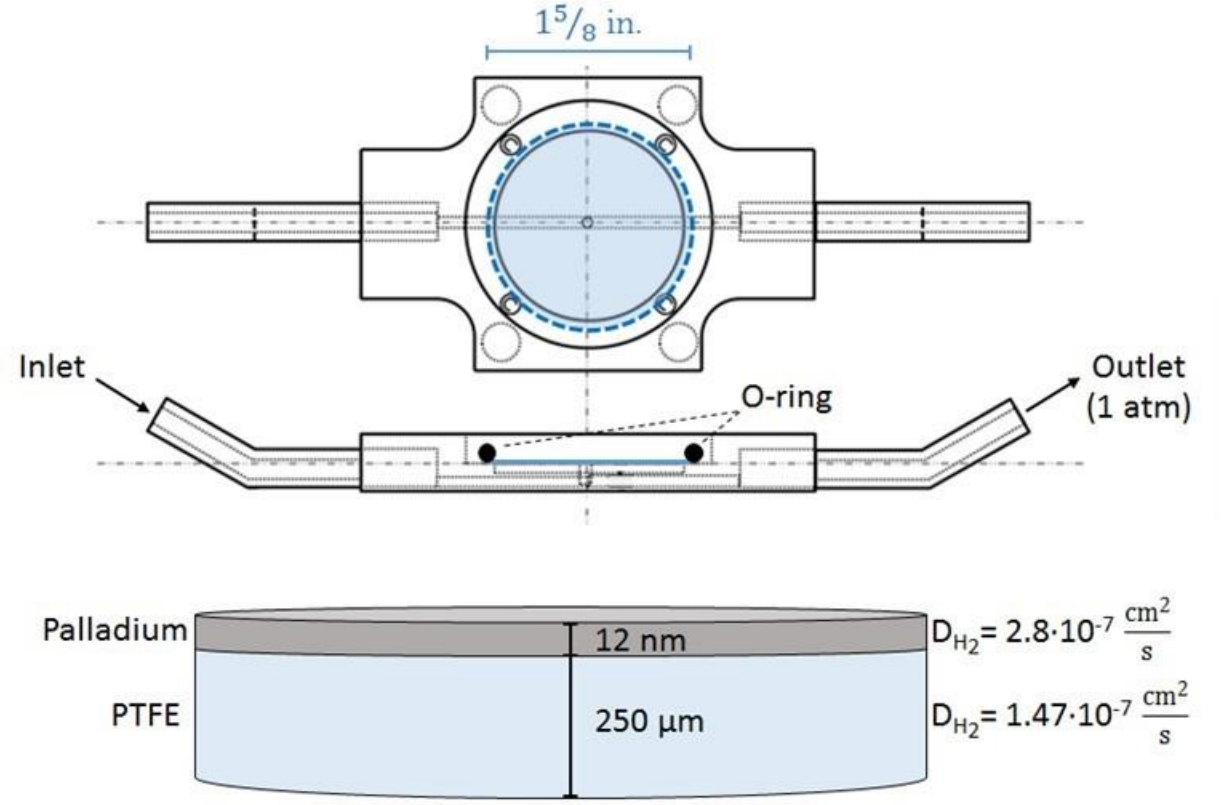

Figure 16. Schematic of the top view (above) and side view (center) of the sample holder used for AFM experiments. H_2 or N_2 gas is supplied to the inlet and flows underneath the sample (bottom) towards the outlet. The gas is supplied to the underside of the sample via the 2 mm diameter central aperture, where it begins diffusing through the sample to the catalyst surface.

To validate the designed sample holder for hydrogen delivery, a colorimetric experiment has been performed. Hydrogen was supplied underneath a PdCl(II) coated polyetherimide (PEI) membrane, and a change in the metal color from brown to silver verifies its exposure to hydrogen. The results of the colorimetric experiment are shown below in Figure 17.

Figure 17. Colorimetric results of the exposure of a PdCl(II) coated PEI membrane supplied with H_2 for 22 minutes using the designed sample holder. The change in color from before (a) to after (b) hydrogen flow demonstrates the sample holder's ability to deliver hydrogen to the underside of the sample, which can then diffuse through the catalyst surface.

For a homogeneous surface, it can generally be assumed that the observations made in one localized area can be representative of the entire surface at that point in time. In that case, over the full duration of the slow scan of a catalytic surface during a chemical reaction, any changes observed are not representative of location, but are instead of the entire surface with respect to time. The left/right serpentine x-direction of the scan is not provided, so the points in these individual lines are instead averaged together to form a single point. Time then progresses in the y-direction as the scan continues, resulting in a plot of phase angle as a function of time. It is valuable to observe both, as the averaging of peaks and valleys present in the 3D landscape can potentially result in loss of data if only viewed on the 2D, time-dependent representation. A simplified diagram of this process is presented in Figure 18 below.

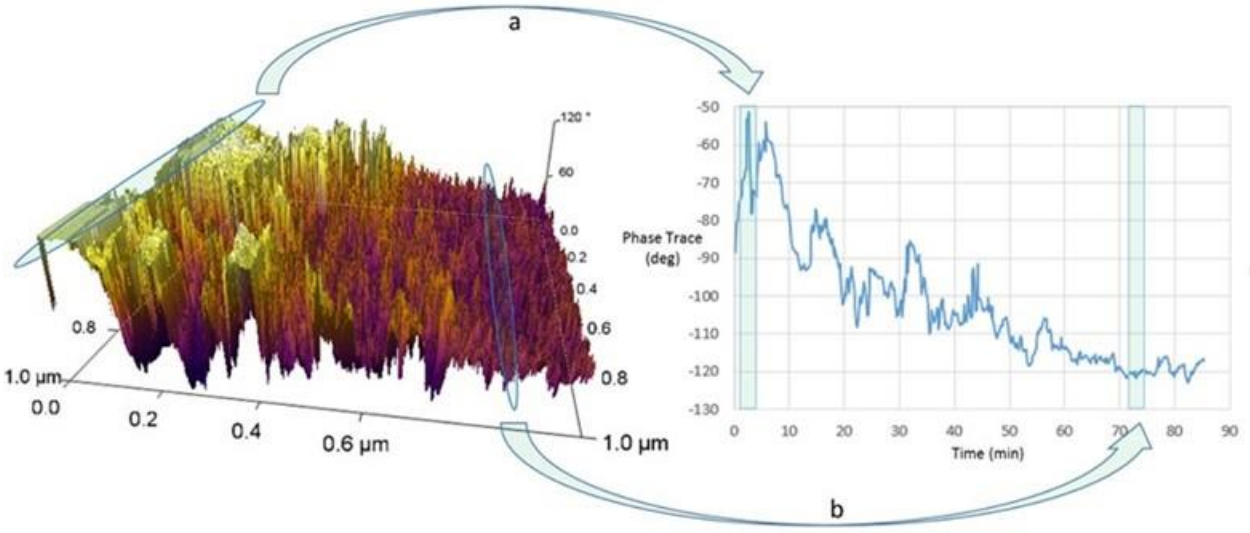

Figure 18. Example of the conversion of a three-dimensional phase angle landscape provided by the Asylum Research MFP-3D instrument operated in AC mode using WaveMetrics Igor Pro 5.0.5.7 software (left) to an x-y plot of phase angle as a function of time (right). The individual lines of data in groups (a) and (b) are averaged together to form their respective points on the x-y plot.

5.2 Untreated PTFE Sample

PTFE was selected for a sample material due its insolubility in phenylacetylene, styrene, and ethylbenzene. It was necessary to verify stable scans on an untreated PTFE surface before moving on to scans sputtered with palladium, if only to ensure that the system can be operated successfully under a liquid reagent. If the phase angle data were to behave differently for a palladium-sputtered surface than for an untreated PTFE film, with the overall system either not changed or changed in a consistent manner, then those differences could also be attributed to the new interactions presented by the palladium surface rather than the subtle signatures of chemical reaction and mass transfer at the liquid-solid interface.

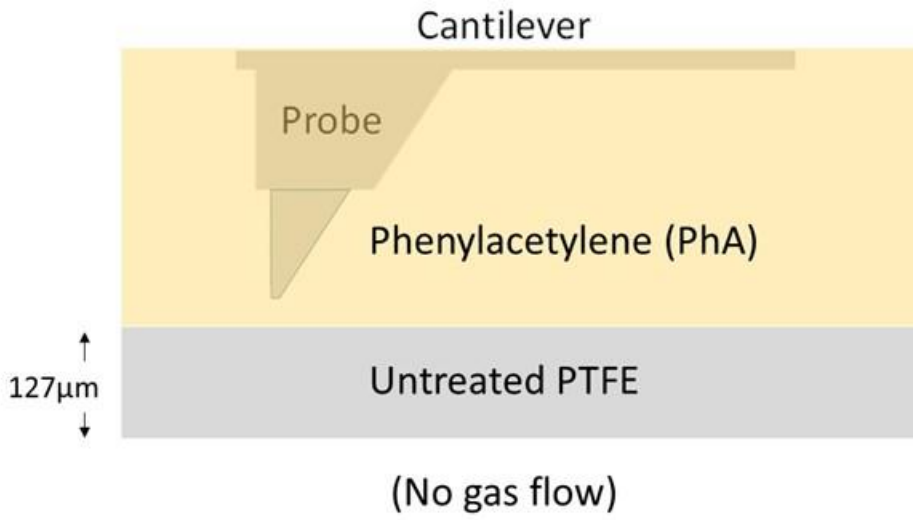

Figure 19. Schematic representation of the AFM system for scanning an untreated PTFE surface with the probe submerged in phenylacetylene.

During attempted scans under phenylacetylene, the liquid temperature and fluid motion after injection appeared to cause phase noise. Phenylacetylene is kept refrigerated for storage, and so it will equilibrate to room temperature after addition to the system. When scans were started immediately after the addition of cold phenylacetylene, the system was unable to be stabilized to gather useful data due to noise. When left to equilibrate for up to three hours, the scans became more stable with time. Phenylacetylene reaches room temperature in approximately 40 minutes, so further equilibration most likely accounts for fluid motion and any potential swelling of the PTFE layer.

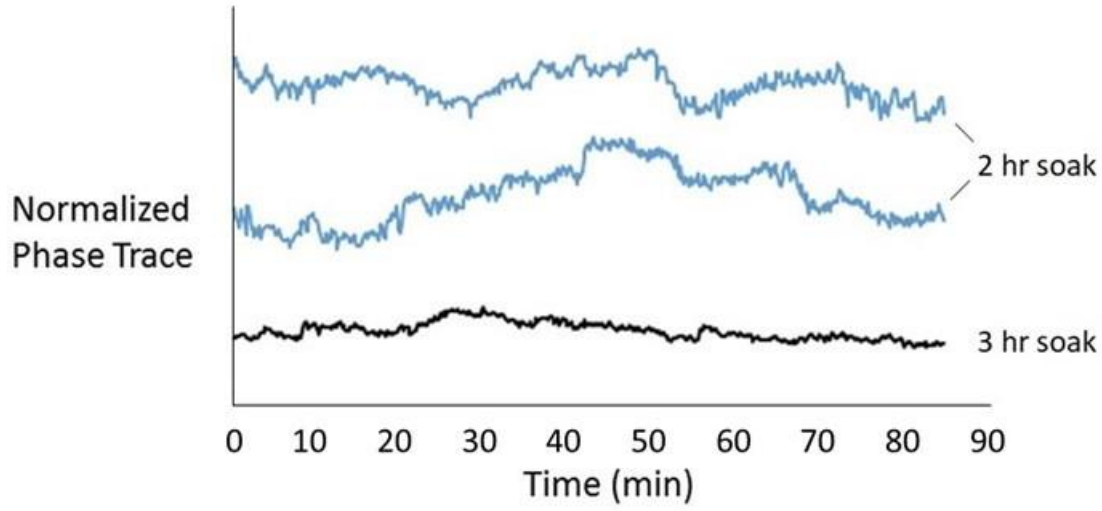

Figure 20. Line-averaged phase trace data for scans of an untreated PTFE surface under phenylacetylene when left to equilibrate for two or three hours. Longer equilibration times appear to reduce noise in the phase trace data.

5.3 Palladium-Sputtered Sample

5.3.1 Hydrogenation of Oxygen Layer to Form Water

The data analysis for the sorption of hydrogen to a Pd-sputtered polycarbonate film surface in water is shown in Figure 21 below. Because the system depends on gas sorption rather than reaction progress, the supply gas is switched between hydrogen and nitrogen to observe the effect the sorbed gas has on the AFM phase data. Nitrogen is not capable of permeating through the Pd layer [42].

Some trends are easily observed. As expected, nitrogen flow generally has no effect on phase angle due to its inability to permeate through the Pd layer. Hydrogen flow causes an increase in phase angle due to changes in interactions with the tip between a sorbed hydrogen layer and a bare palladium surface. Less obvious, and more crucial to validate the use of AFM for observing a hydrogenation reaction, is the presence of a slight dip shortly after the *first* start of hydrogen flow

(circled in blue), which is then absent or smaller in magnitude upon the second. This seems to indicate that this dip in phase angle is due to the initial presence of a chemisorbed oxygen layer on the palladium surface, which is reacted with the initially permeated hydrogen to form water and then desorb from the surface into the bulk.

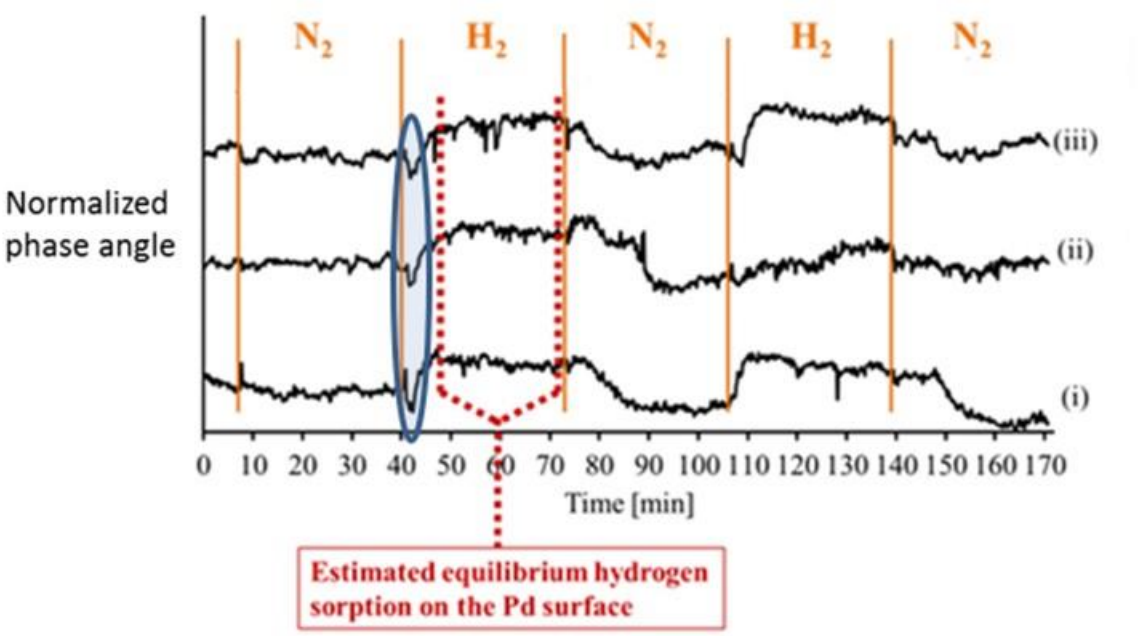

Figure 21. AFM phase angle data for the hydrogen permeation of a 250 μm thick, Pd-sputtered polycarbonate film. The dashed red lines indicate the calculated time range for hydrogen saturation of the PC film [23]. The dip in phase angle within the blue circle represents the hydrogenation of the oxygen layer to form water.

This observation serves to illustrate the potential innovation of using AFM to observe the time-dependent change in surface chemistry that takes place over the course of a catalytic membrane reaction. This will be strengthened by observation of the catalytic hydrogenation of phenylacetylene using AFM. With recent interest in producing AFM hardware capable of high pressure and temperature (many atmospheres, several hundred °C) [43] , the ability to use AFM

to observe surface chemistry in real time during reaction at industrially relevant reaction conditions may be significantly broadened.

5.3.2 Scanning with Permeating Hydrogen and Nitrogen

To observe the effects of gas flow on phase noise, scans were performed with nitrogen and hydrogen flow as noted in Figure 23. The ordinate has been normalized to facilitate comparison. Since no palladium catalyst layer is present, the only difference in the system caused by a gas switch will be the diffusion of H_2 or N_2 through the Teflon film.

Table 8. Diffusion coefficients for hydrogen and nitrogen in PTFE at 25°C.

Gas	**D (cm^2/s)**
H_2	$1.47 \cdot 10^{-7}$ [34]
N_2	$0.88 \cdot 10^{-7}$ [44]

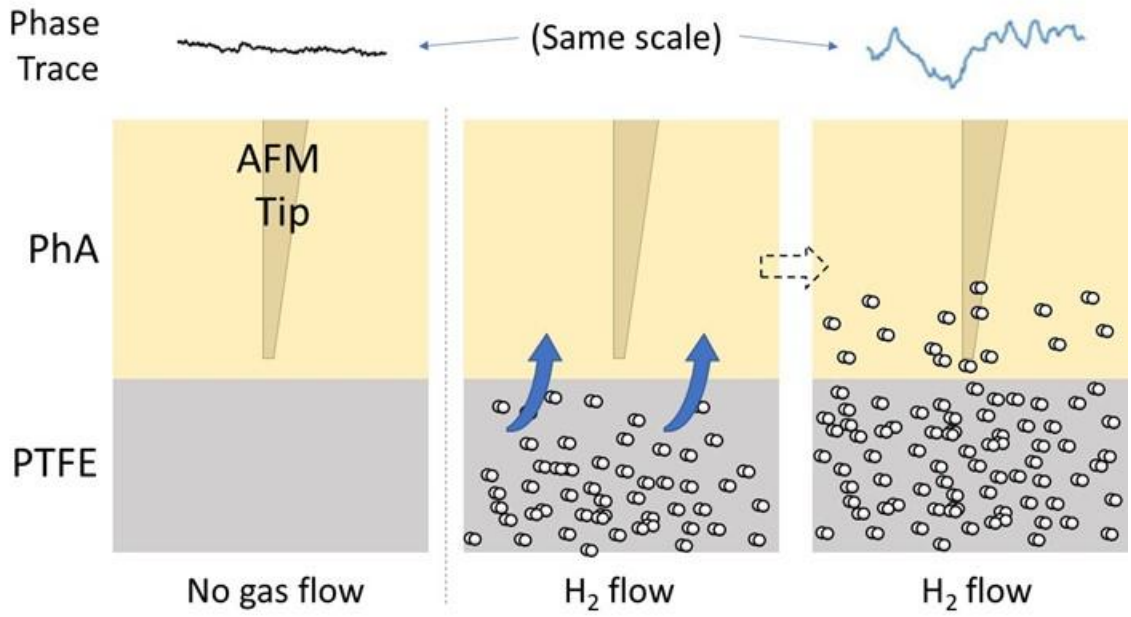

Figure 22. Depiction of H_2 gas permeation through a PTFE film, causing phase noise as it diffuses around the AFM tip.

For each gas, there is considerably more noise in the phase trace plot than either of the two-hour or three-hour equilibration scans without gas flow in Figure 20. Neither H_2 nor N_2 should interact with the AFM probe, so their effect on phase trace is expected to be due to physical and not chemical interaction. It is possible that the noise is the result of vibrations in the gas supply line, which would be indiscriminate to the type of gas being supplied. As the gas diffuses through the PTFE film to the surface, the appearance of the gas at the surface near the probe tip and subsequent diffusion into the nearby surrounding liquid could potentially add further noise. This effect may also be proportional to the diffusion rate of the gas, and so hydrogen would be expected to have a greater impact than nitrogen.

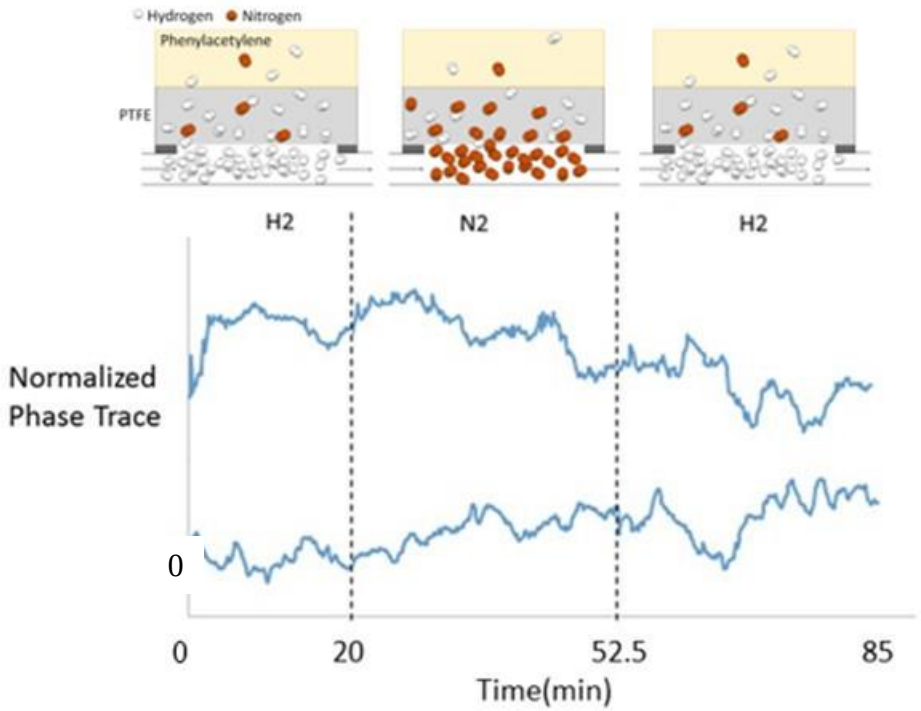

Figure 23. Two normalized scans of an untreated Teflon surface (no Pd coating) exposed to $H_2/N_2/H_2$. The diffusion of gas to the sample surface appears to create additional noise when compared to the scans of Figure 20 without gas flow. Valve switching only appears to affect AFM data at the point of valve manipulation, visible as a small spike in phase trace. Any short-term impact is also dampened by the averaging performed to obtain the line graphs (Figure 18).

5.3.3 Scanning on Palladium Sputtered on Teflon

After performing scans of an untreated PTFE sample in PhA with H_2/N_2 flow, the next step was to repeat the scan on a catalytic Pd surface sputtered onto the Teflon. H_2 flow was initiated 30 minutes prior to the three-hour equilibration period to provide time for hydrogen to dissociate and diffuse to the catalyst surface. Without hydrogen on the surface the reaction can be considered hydrogen starved, which may lead to potential fouling or deactivation of the catalyst. During warmup and for the first period of hydrogen flow, H_2 permeates through the PTFE sample to the Pd layer, where it dissociates into monoatomic hydrogen and diffuses through the metal to the surface. When switched to N_2, a hydrogen concentration gradient forms across the sample, facilitating diffusion from the fluid and surface back through the sample towards the nitrogen side. As hydrogen diffuses away from the surface layer, it can be resupplied by hydrogen from the bulk PhA and the PTFE film. When switched back to hydrogen flow, the remaining N_2 diffuses out of the PTFE into the bulk gas. Hydrogen diffusion occurs as before until the surface is again saturated.

Figure 24**Error! Reference source not found.** shows two separate scans of the Pd surface during the hydrogenation of PhA. Since hydrogen has been flowing for over three hours prior to the start of the scan, it can be assumed that little change should be observed during the first 20 minutes of continued H_2 flow. Some phenylacetylene will have converted to styrene and ethylbenzene, shown in the smaller schematics above. Aside from set point adjustments at the beginning of the scan (observed as noise at the start of the top scan), the phase angle behavior is somewhat consistent between the scans. Both scans are relatively stable during the first period of H_2 flow, due to diffusion having approached steady state after a long soak period. After switching to N_2 flow, the plots of phase angle differ, but show an overall decrease in phase prior to the switch

back to H_2. After 10-12 minutes of hydrogen flow, the phase angle begins to increase. Both trends follow those also observed in the previous work presented in Figure 21.

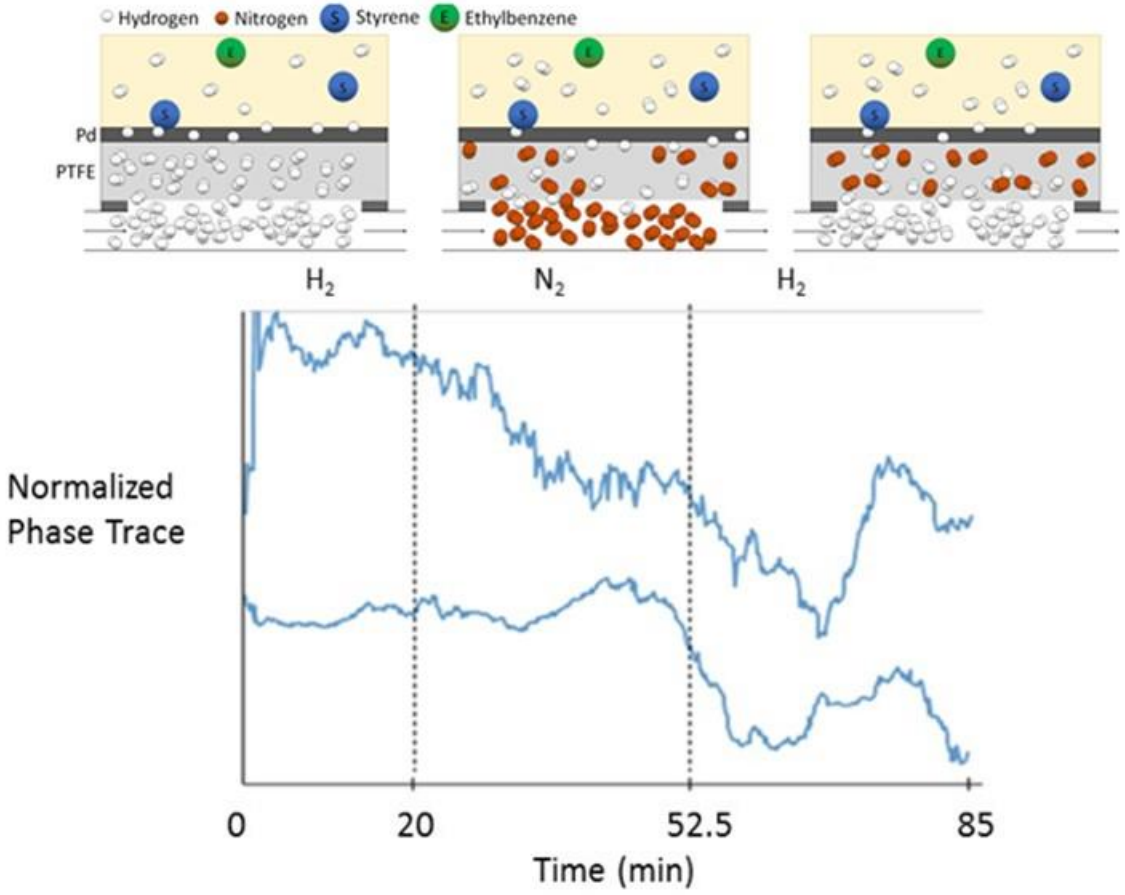

Figure 24. AFM data for the hydrogenation of phenylacetylene using gas switching. Hydrogen was flowing for three hours prior to scanning, and for the first 20 minutes of the scan. Gas flow was switched from H_2 to N_2 for the next 32.5 minutes and switched to H_2 for the final 32.5 minutes.

5.4 Styrene Immersion with Ethylbenzene Injection

To simulate an accelerated reaction, styrene was used as the immersion liquid and injected with ethylbenzene. After hydrogen is introduced and begins to reach the solid-liquid interface, styrene molecules from the bulk fluid should begin to adsorb to the catalyst surface. Since styrene interacts with the surface hydrogen and ethylbenzene does not, it was assumed that the addition of ethylbenzene to the bulk fluid would not change the interactions observed at the interface. A schematic representation of this effect is shown below in Figure 25.

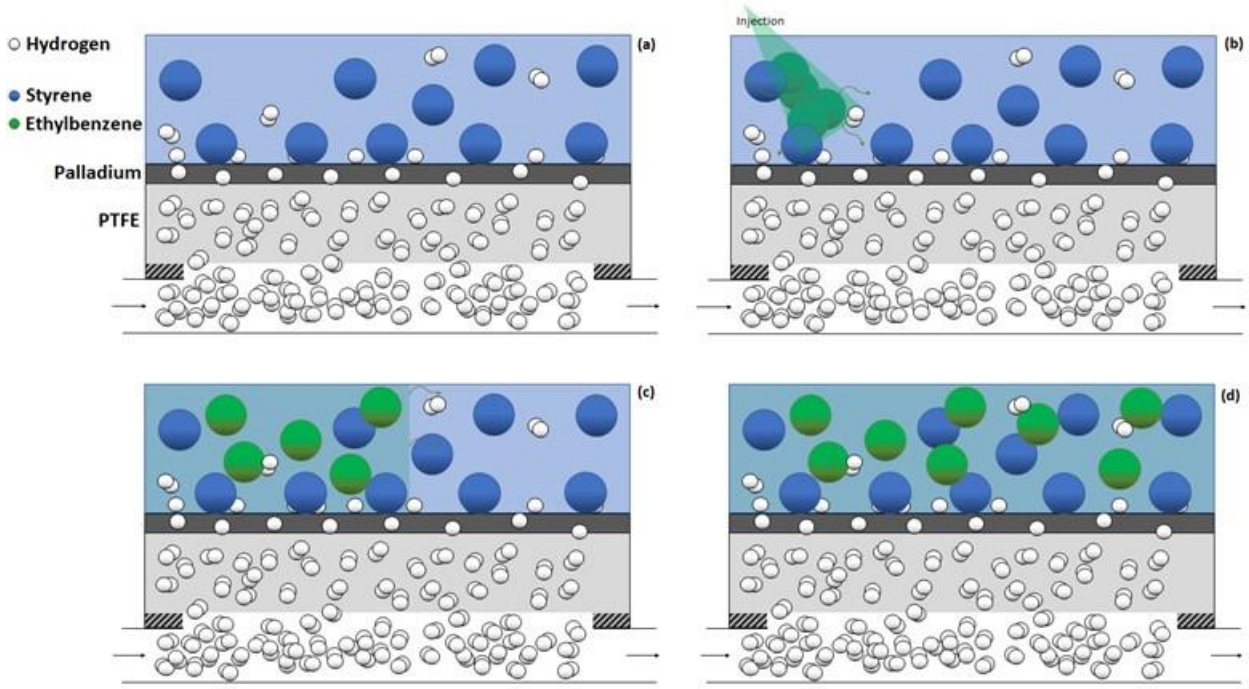

Figure 25. Injection of ethylbenzene into a styrene-Pd system. Styrene is initially adsorbed to the Pd-H catalyst surface (a). Ethylbenzene is injected into the bulk fluid (b) but is already saturated and does not interact with the surface. Ethylbenzene diffuses into the bulk (c and d) but is not expected to strongly affect the chemistry at the catalyst-liquid interface.

In Figure 26, hydrogen flow is initiated at the 10-minute mark and the phase trace again begins to trend upward as expected. 0.3 mL ethylbenzene is injected at the 32-minute mark. Rather than having no effect on the phase trace plot as in the EB medium scans, there is instead a

slight positive jump before the phase trace dissipates. The spike in phase trace is most likely due to physical agitation of injection, and so as the liquid around the cantilever begins to settle again, phase trace is observed slowly drifting back down to the baseline value seen prior to injection. This follows the hypothesis that while the styrene interacts with the catalyst surface, the ethylbenzene merely diffuses into the surrounding bulk and does not change the surface chemistry. After the transient subsides, only the bulk fluid has changed, and the probe observes no significant difference on the surface.

40 minutes after injection, the gas is again switched from hydrogen back to nitrogen. As hydrogen leaves the surface to diffuse into the bulk liquid and down through the sample, the reaction can be viewed as "switched off". Though the phase angle increases after the switch, opposite of the expected trend, this change is instantaneous rather than gradual and so is most likely due to the mechanical agitation of valve manipulation.

A similar trend is observed in Figure 27. Nitrogen flow is initiated below a styrene-palladium sample and is switched to hydrogen at ten minutes. While the phase trace does not begin to increase after the gas switch as observed previously, the slope of the baseline does become more positive. At 30 minutes, 0.5 mL ethylbenzene is injected into the system. Despite the larger volume of injection, the positive spike in phase trace is smaller than injections of a lesser volume. This may be due to subtle differences in injection conditions caused by human error, such as injection rate or location. After the injection transient subsides, however, the phase trace begins to stabilize at a value lower than the baseline observed prior to injection. This could be due to subtlety of numerous factors which can impact phase data, or may indicate that as the reaction progresses from styrene to ethylbenzene, a decrease in phase angle could be expected. Since the same trend was not observed in Figure 26, further scanning must be performed.

After the 50-minute mark, the phase trace gradually increases as expected with hydrogen flow. When switched back to a nitrogen supply, the phase trace immediately begins decreasing. This coincides with the trends observed in previous work, as well as in the data presented here.

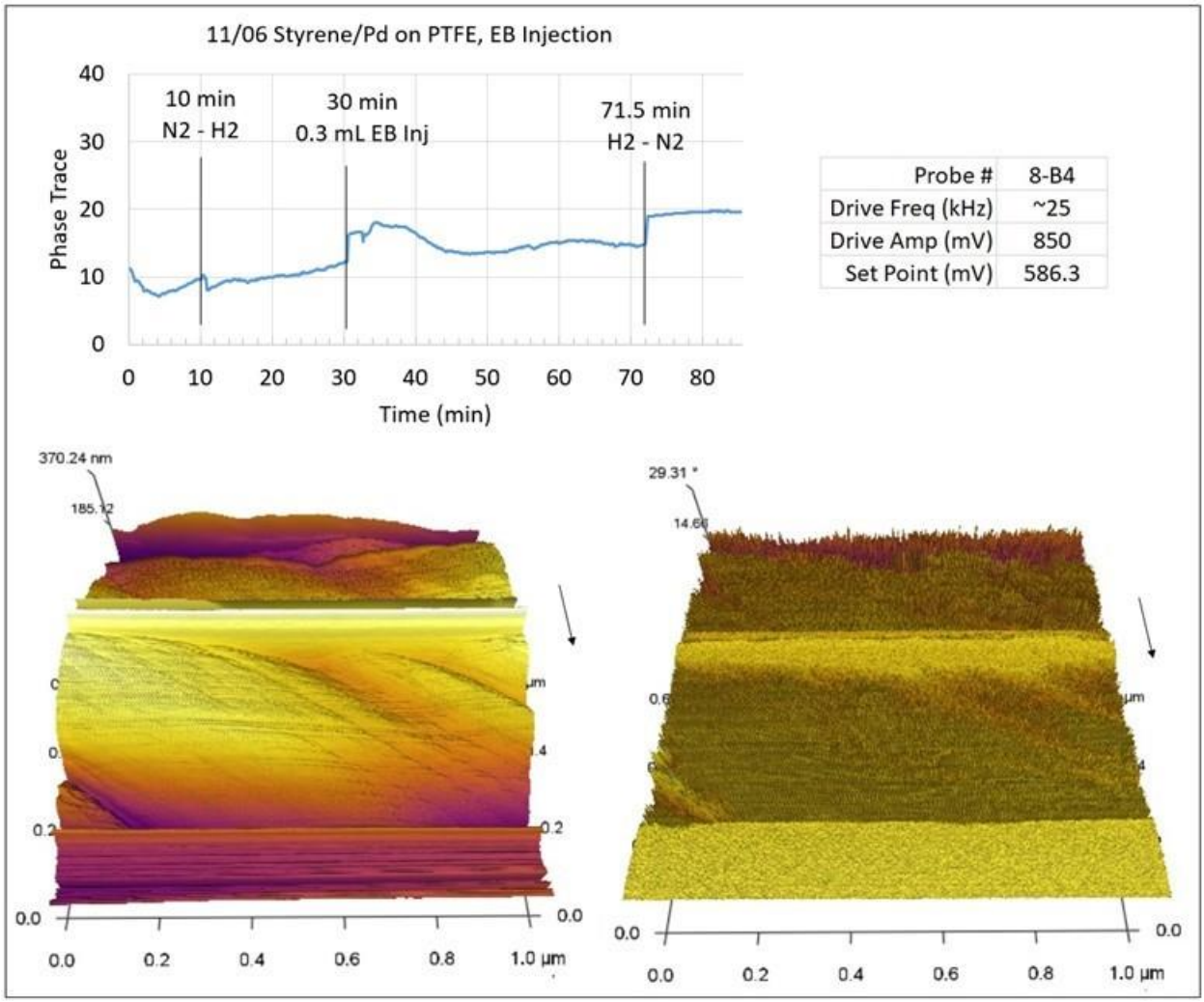

Figure 26. Styrene on palladium with 0.3 mL EB injection, scanning frequency ~ 25 kHz. Phase trace is plotted with respect to time (top). 3-dimensional images of height (left) and phase (right) are shown for one complete scan. Arrows represent scan direction.

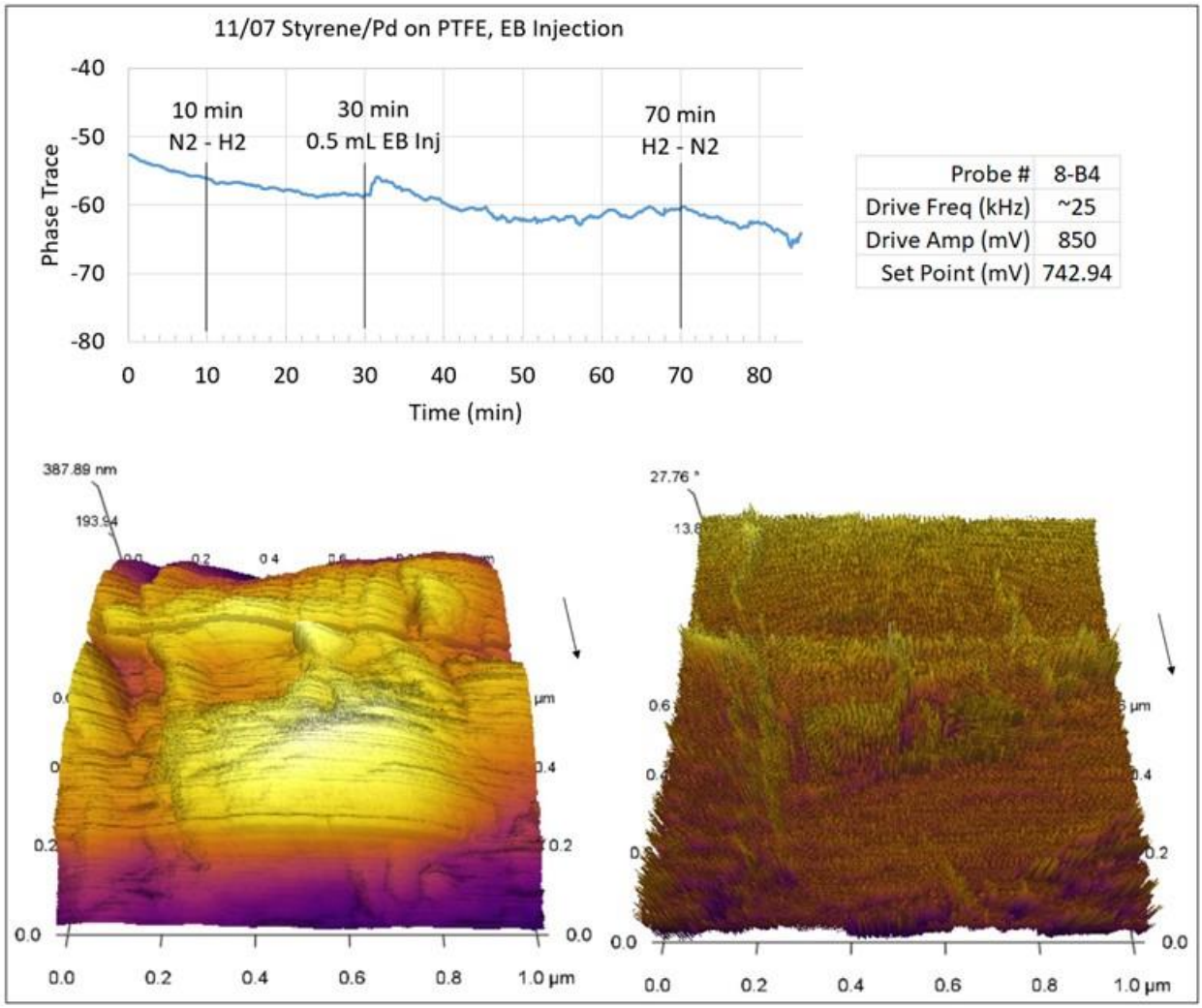

Figure 27. Styrene on palladium with 0.5 mL EB injection, scanning frequency ~ 25 kHz. Phase trace is plotted with respect to time (top). 3-dimensional images of height (left) and phase (right) are shown for one complete scan. Arrows represent scan direction.

Figure 28 closely follows the same initial phase trace trends observed previously. A dip in phase trace indicates the formation of water after hydrogen flow is started. The phase trace data is relatively calm until the ethylbenzene injection, at which point there is a transient that eventually stabilizes. However, the phase shift again stabilizes at a value lower than the baseline observed prior to injection. When hydrogen flow is switched back to nitrogen, there is a mechanical shock and immediate, slight increase in phase.

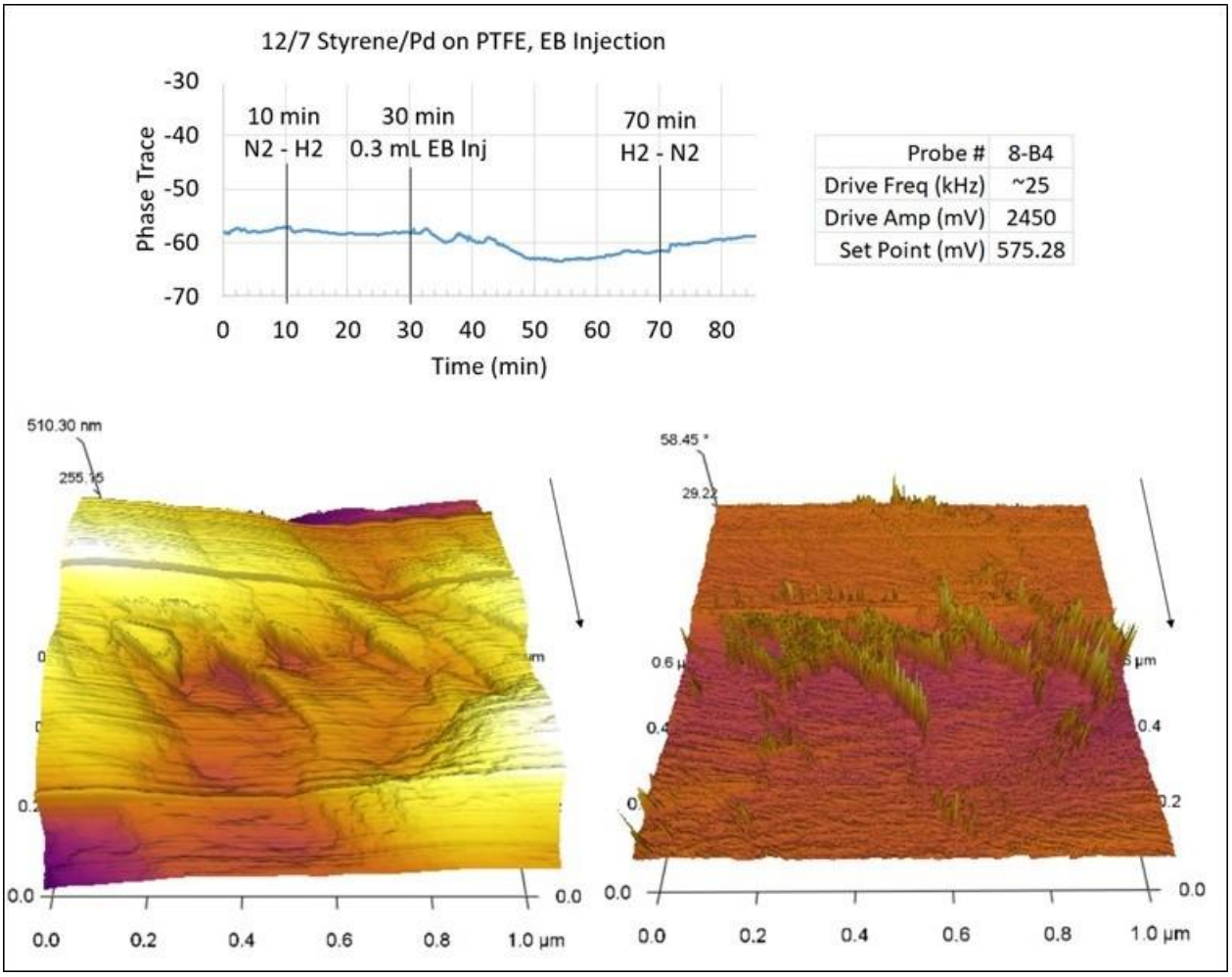

Figure 28. Styrene on palladium with 0.3 mL EB injection, scanning frequency ~ 25 kHz. Phase trace is plotted with respect to time (top). 3-dimensional images of height (left) and phase (right) are shown for one complete scan. Arrows represent scan direction.

Important to note for comparison below is that in all three scans, ethylbenzene was not expected to have a lasting impact on the phase angle data due to it being the final hydrogenation product in the phenylacetylene reaction pathway. It is not expected to interact with the catalyst surface, however the phase data after ethylbenzene injection stabilized at a value slightly below baseline in two of the three scans. For more clarity, the reverse case will be observed in chapter 5.5, with styrene injections into an ethylbenzene-immersed system.

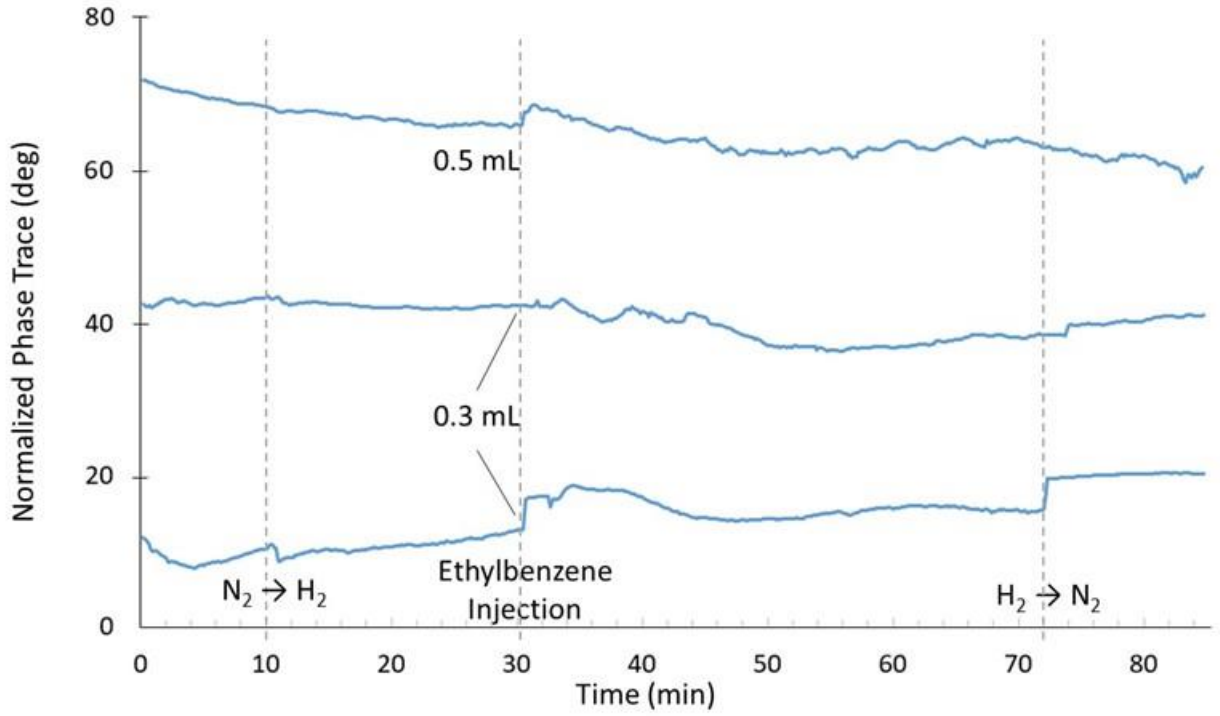

Figure 29. Normalized phase trace plots for AFM scans of a PD-sputtered PTFE surface immersed in styrene.

5.5 Ethylbenzene Immersion with Ethylbenzene and Styrene Injections

Ethylbenzene (EB) is the final hydrogenation product in the reaction chain of phenylacetylene (PhA) to styrene (St) to EB. Were the reaction to be conducted to 100% conversion under AFM, it is assumed that the phase trace would start at some constant value representing the interaction between a sorbed PhA-Pd surface and the cantilever tip. As the PhA is hydrogenated to St and finally EB, the phase trace would be expected to eventually stabilize at some lower, constant value when only EB is present.

Since ethylbenzene is not expected to strongly sorb to the catalyst surface and no other chemicals should be present after the reaction is complete, the addition of more ethylbenzene should not affect the phase trace in a manner associated with the interactions present between the tip and the sample. In the reverse case from section 5.4, the injection of styrene into an

ethylbenzene immersed system is expected to be visible under AFM. As styrene is introduced to the catalyst surface, it will interact with any active hydrogen sites to adsorb to the catalyst surface and hydrogenate to ethylbenzene. This change in surface chemistry should be reflected as a change in the phase trace data, and a schematic of the liquid-solid interface during this transient is shown below.

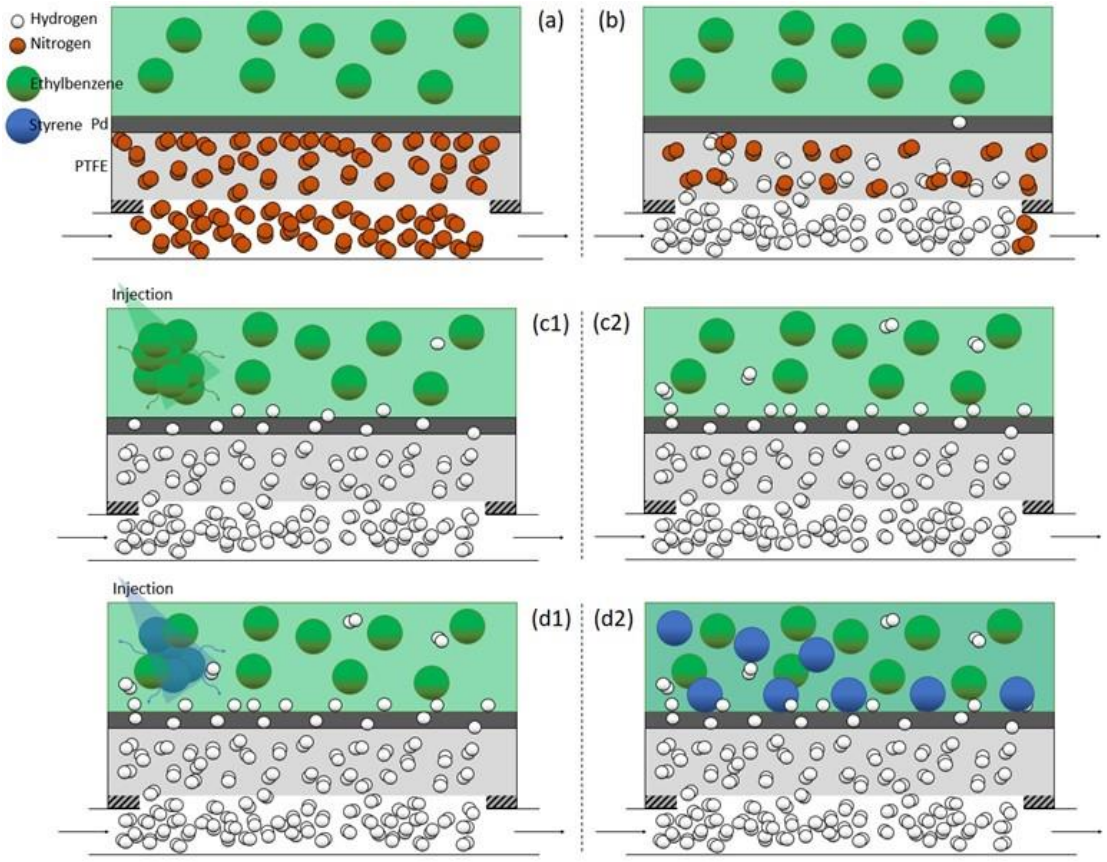

Figure 30. Schematic diagram of the ethylbenzene system transients. In part (a), nitrogen is supplied and diffuses into the PTFE layer. Ethylbenzene is stagnant at the surface. In part (b), the nitrogen supply is switched to hydrogen. Ethylbenzene and styrene are injected in parts (c) and (d), respectively.

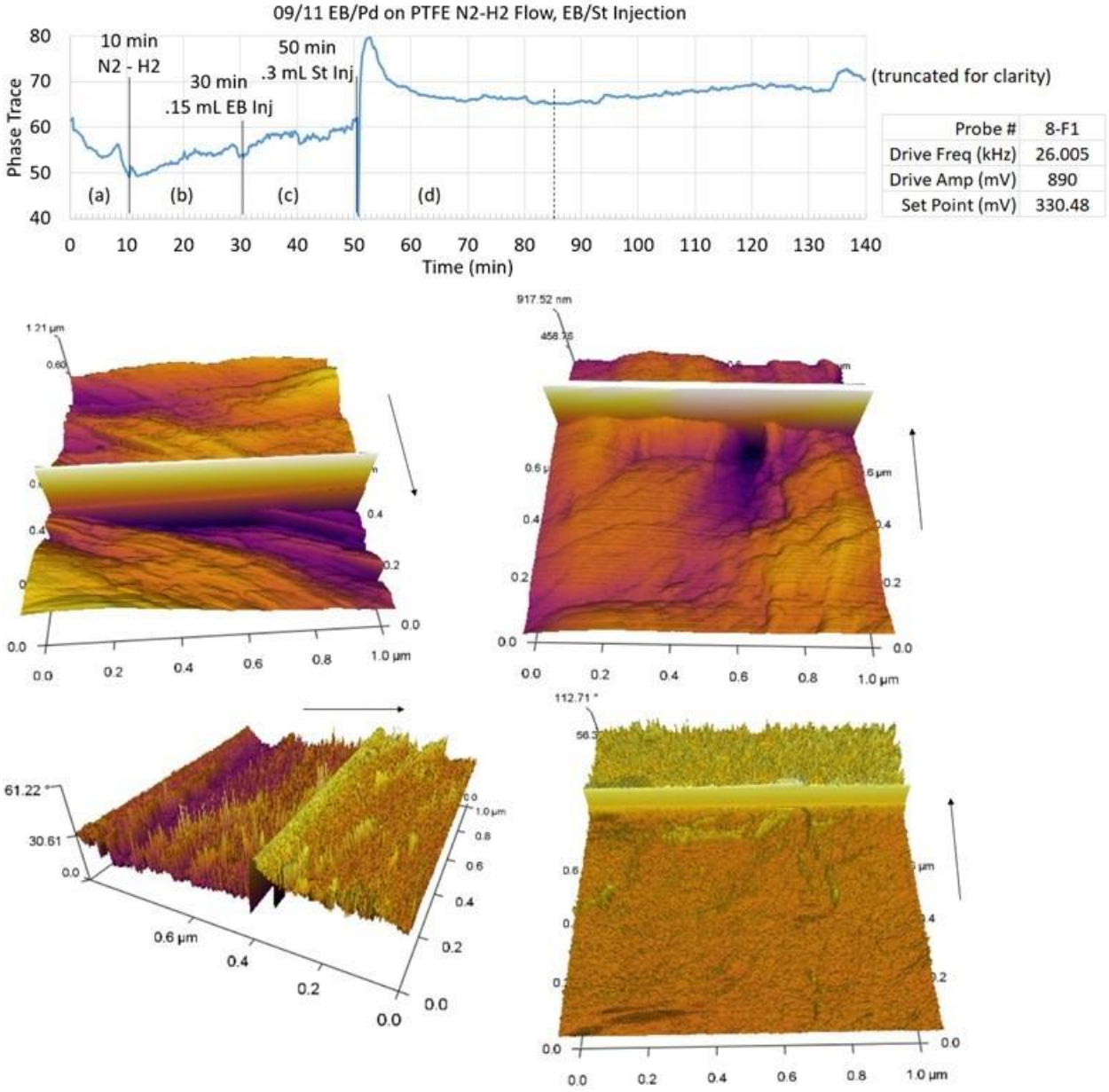

Figure 31. Ethylbenzene on palladium with EB and St injections, scanning frequency = 26 kHz. Phase trace is plotted with respect to time (top). 3-dimensional images of height (middle) and phase (bottom) are shown for two complete scans. Dotted line at 85 minutes represents change of scan direction. Arrows represent scan direction.

In Figure 31, a scan has been performed over a palladium-coated Teflon film immersed in ethylbenzene. As before, after 10 minutes of scanning the nitrogen is shut off and hydrogen flow

is initiated, with the corresponding drop in phase trace for water formation and a gradual increase in phase as hydrogen appears at the surface. The ethylbenzene molecules are not expected to interact with the sorbed hydrogen, so any changes in the phase trace at this point are expected to only be due to the appearance of hydrogen.

At the 30-minute mark, 0.15 mL of ethylbenzene is injected into the system approximately 1.0 cm from the AFM probe. The phase trace is expectedly unaffected by the injection and continues the same upward trend due to hydrogen permeation.

At the 50-minute mark, 0.30 mL of styrene is injected. The mechanical shock of the injection can be observed as the immediate negative spike in phase trace. To differentiate chemical shock from physical shock, equal volumes of EB and St were injected in a scan described later. The large positive spike in phase trace again occurs two minutes after the injection and takes an additional six minutes to dissipate. This is once again attributed to the agitation of the liquid medium, which then takes time to settle and become stagnant. This behavior is similar to when first adding liquid to immerse the cantilever, when the system is left to equilibrate for 15-30 minutes until the Sum signal stabilizes. The cantilever has already been exposed and calibrated to the liquid medium long before the injection, so it makes sense that the transient following the injection is shorter than for the initial immersion. It is also noteworthy that after the styrene transient subsides, the phase trace remains relatively constant. Because the mass transfer of hydrogen to the catalyst surface is so slow (Section 4.2), it is not feasible to observe the progression of the reaction in real time using AFM in this reaction system. This means that once the catalyst surface is saturated with styrene-hydrogen (St-H) interactions, it would be expected to remain so for the remainder of the scan. While some styrene will convert to ethylbenzene, this will most likely not be observable due to three main factors:

1. The AFM probe may not be present at the reaction site at the time of conversion (unlikely due to reactions occurring on timescales as small as femtoseconds).
2. If the probe is at the reaction site, the data point will not significantly change the average of the entire line of data.
3. The change in phase trace value may not be significant enough between data points to notice relative to general phase trace variance in any one scan.

Though the phase trace is constant after the styrene injection transient, it is also settled at a higher baseline value than before the injection. It is hypothesized here that the increase in phase trace represents the change from a H-Pd saturated surface to a St-H-Pd surface. If this is true, then the reverse should also apply where the conversion of styrene to ethylbenzene would result in a decrease in phase trace.

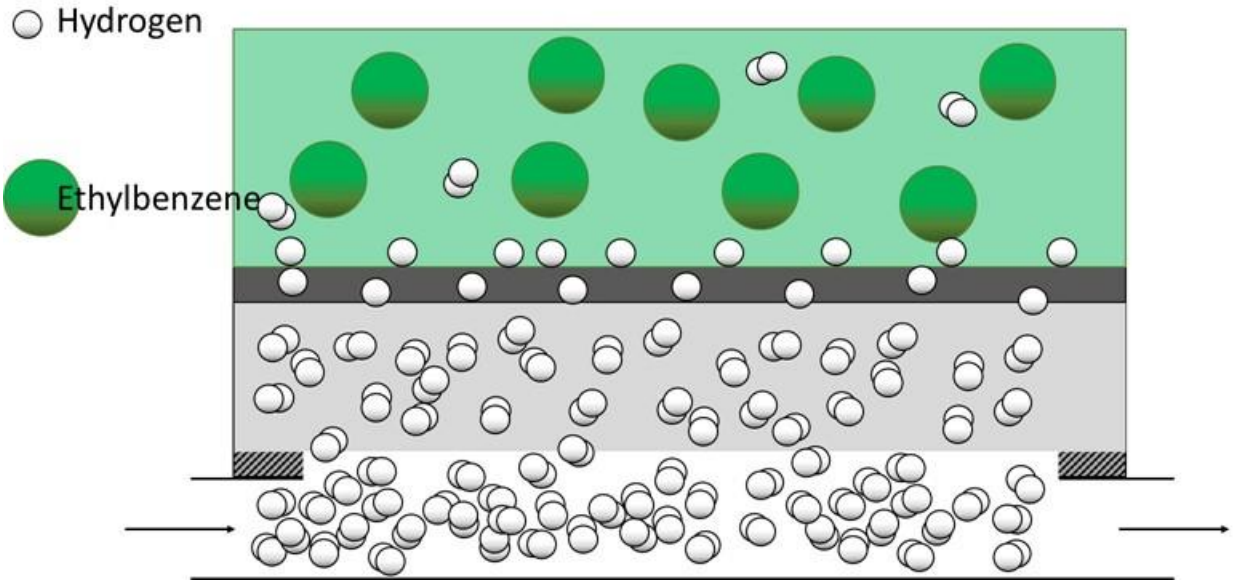

Figure 32. Ethylbenzene system with hydrogen. Hydrogen flows through the supply tube below and has permeated the Teflon and palladium layers. Monoatomic hydrogen appears at the metal-liquid interface. Ethylbenzene does not interact with the sorbed hydrogen. The introduction of more ethylbenzene will not change the chemistry of the system.

Figure 33 below represents an identical process to the scan shown in Figure 31. After the switch from nitrogen to hydrogen, water is formed, and the phase angle eventually begins to increase.

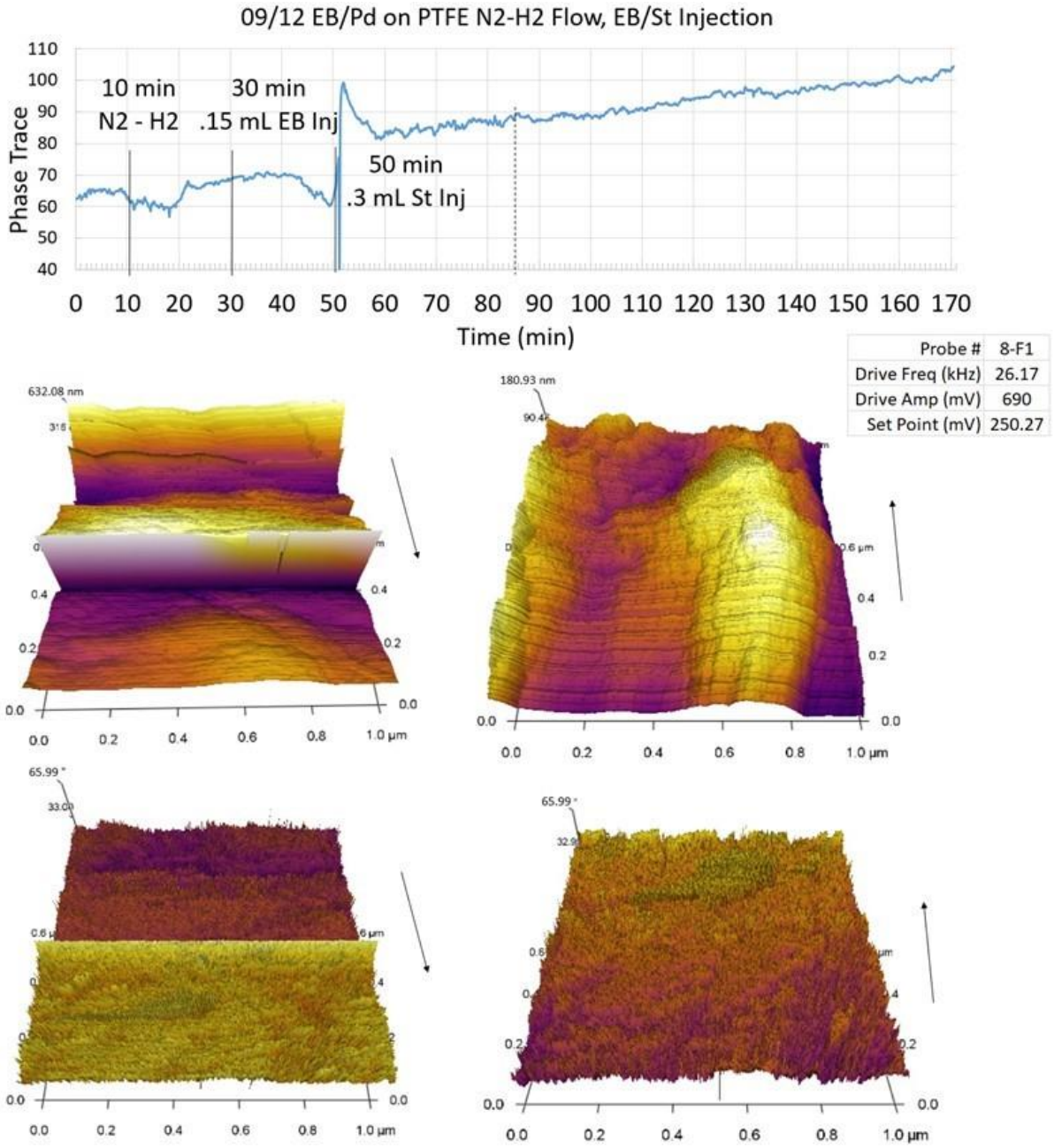

Figure 33. Ethylbenzene on palladium with EB and St injections, scanning frequency = 26 kHz. Phase trace is plotted with respect to time (top). 3-dimensional images of height (middle) and phase (bottom) are shown for two complete scans. Dotted line at 85 minutes represents change of scan direction. Arrows represent scan direction.

The 0.15 mL ethylbenzene injection once again does not affect the phase. At the 50-minute mark a 0.30 mL injection of styrene again results in a large negative spike, followed by a positive peak that dissipates after several minutes and results in a higher baseline value than prior to the injection. This supports the hypothesis that the St-H-Pd interaction results in a higher phase angle than the Pd-H surface.

Figure 34 below represents the same process, but instead uses equal 0.15 mL injection volumes for both ethylbenzene and styrene. The nitrogen-hydrogen switch again results in the formation of water and a gradual increase in the phase trace, and the ethylbenzene injection shows no significant impact. For the 0.15 mL styrene injection, however, the large, negative phase trace observed for the larger volume injections is not present. This may be due to a smaller volume not presenting as large of a mechanical shock to the system. The positive spike is observed, but is smaller than in the 0.30 mL injections and dissipates more rapidly. It may be that the smaller styrene volume does not adequately cover the surface upon injection like the larger injections and must diffuse through the liquid to reach the surface. This could be due to the act of injecting a larger volume causing a greater mixing action within the bulk fluid, reducing the need for longer diffusion times. Like before, phase trace reaches a higher value than prior to the injection and becomes somewhat stable for the remainder of the scan.

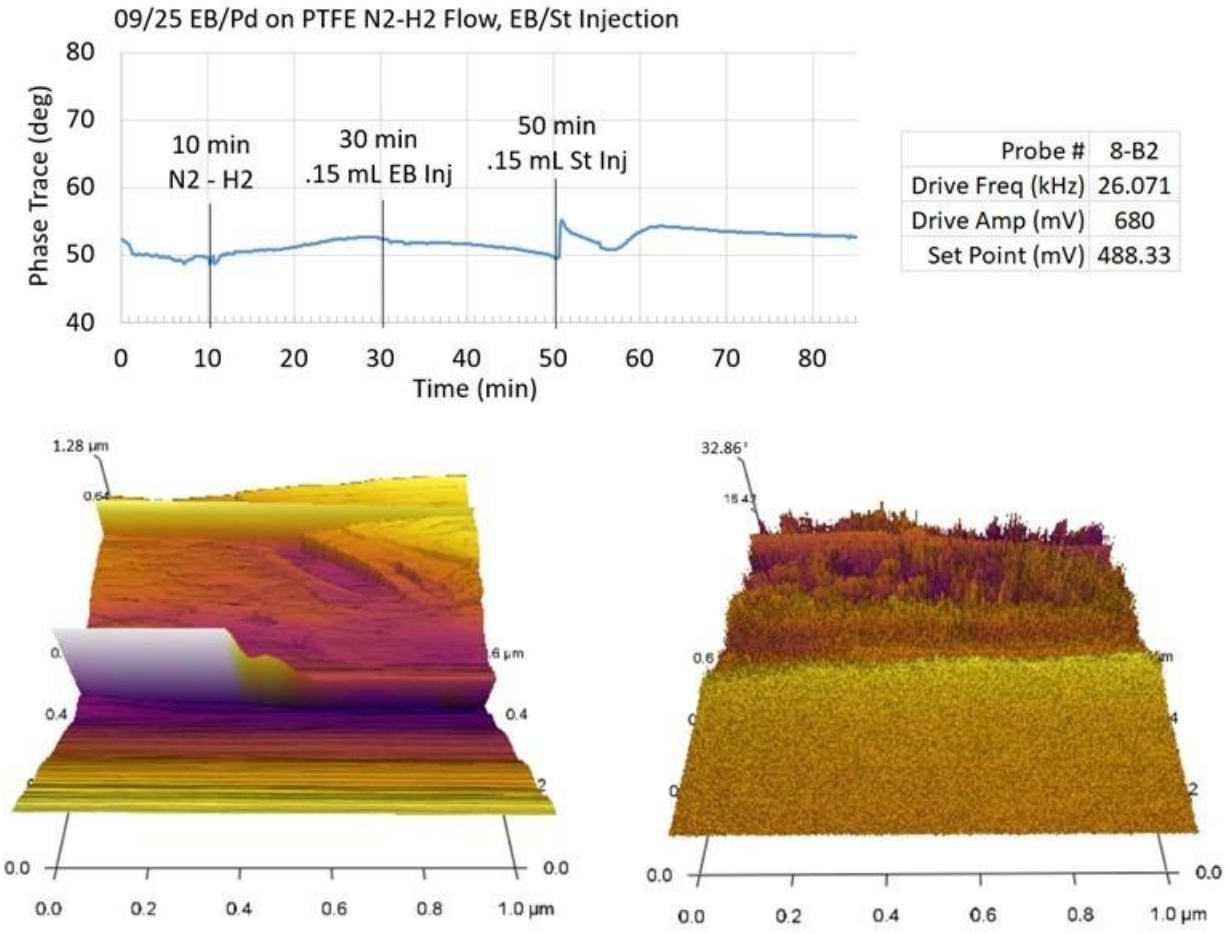

Figure 34. Ethylbenzene on palladium with EB and St injections, scanning frequency = 26 kHz. Phase trace is plotted with respect to time (top). 3-dimensional images of height (left) and phase (right) are shown for two complete scans. Arrows represent scan direction.

The observations made above are much more easily observed as trends when all three scans are plotted together, as in Figure 35 below.

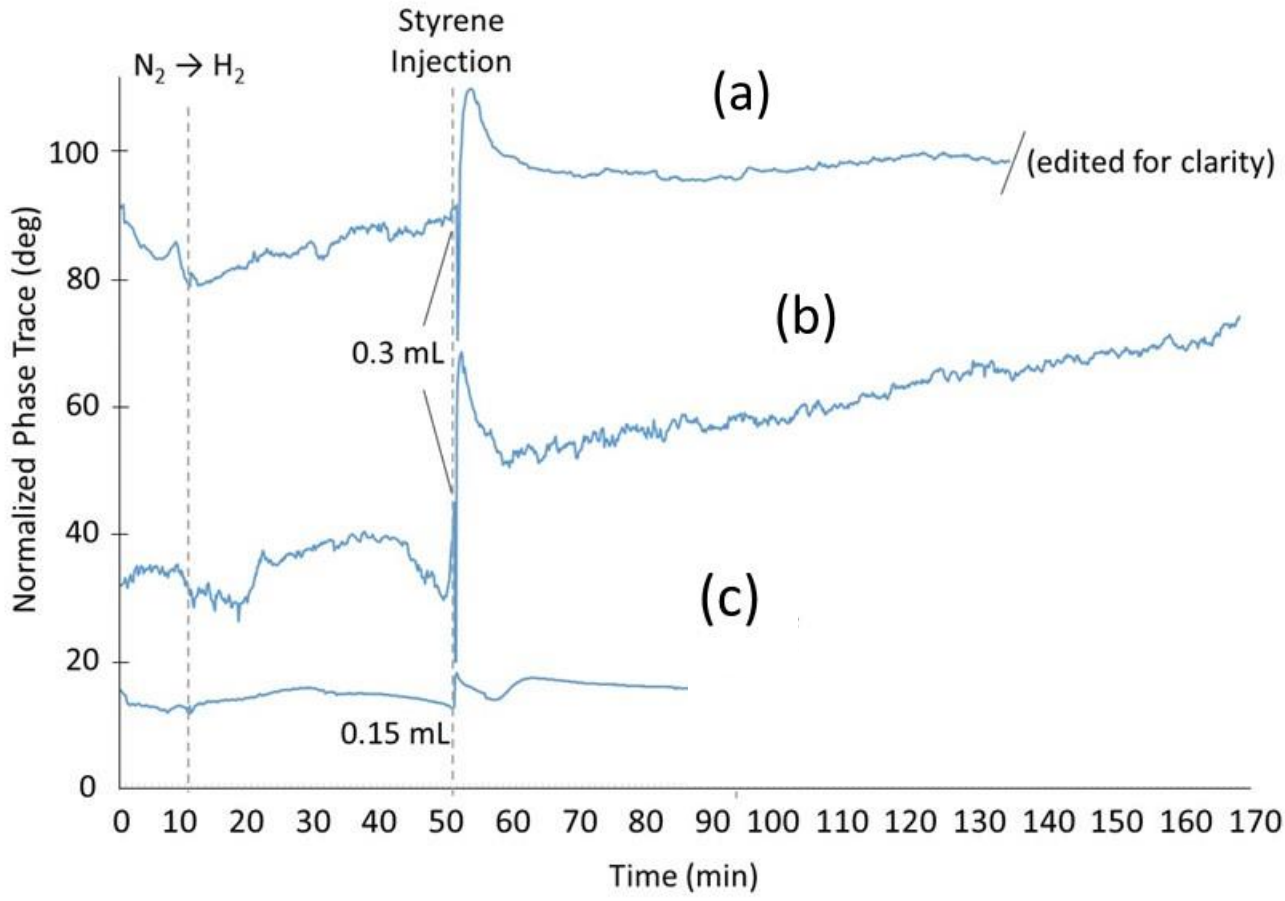

Figure 35. AFM phase trace results for scans on a Pd-sputtered PTFE sample immersed in ethylbenzene.

Shortly after hydrogen flow is initiated, the decrease in phase trace signifies the hydrogenation of the oxygen monolayer to form water. This is consistent through the liquid scans and corresponds to the observations made in previous work [23]. This section of the phase trace data has been enhanced for visibility and is displayed in Figure 36.

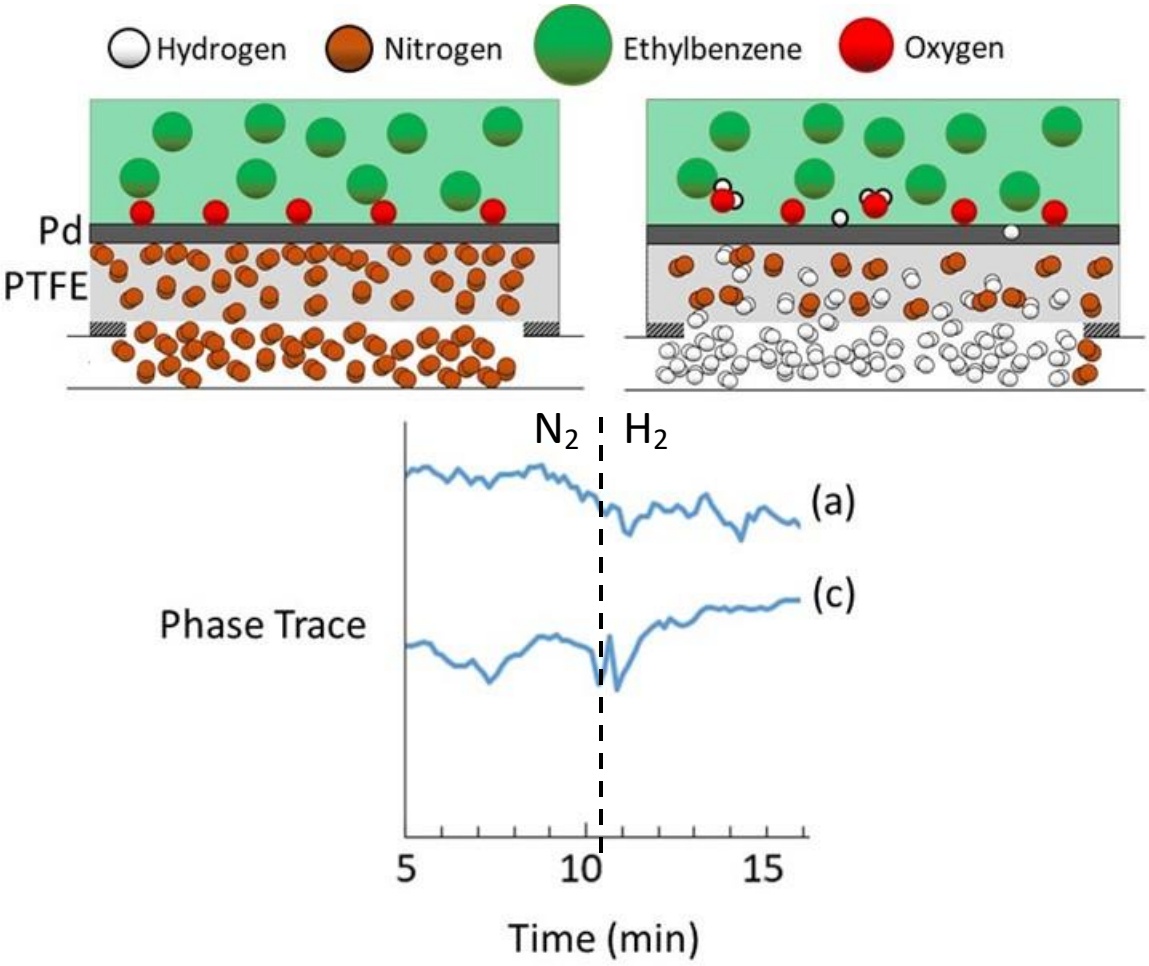

Figure 36. Phase trace data for scans (a) and (c) from Figure 35at the time of gas switching. The shape of the plot of scan (b) makes it difficult to observe this trend, and so that data set has been omitted. The dotted line represents the moment the supply gas was switched from nitrogen to hydrogen. Scan (c) is zoomed in further for readability. Shortly after hydrogen is introduced, the oxygen layer is hydrogenated and removed as water.

What should be gathered from this data set is that the injection of styrene into ethylbenzene causes a large positive spike in phase trace and appears to be proportional to volume of injection. More importantly, even after the phase trace has stabilized it remains at a value that is significantly higher than prior to the styrene injection. This is most likely due to the change in surface chemistry caused by introducing a molecule that interacts with the sorbed hydrogen. This signifies for the first time that AFM can be used to observe the liquid-solid interface during a hydrogenation membrane reaction.

6 Impurities on the Sample Surface

While line averaging is useful for easily interpreting 3D data on a uniform surface, the 3D plot can also be a valuable tool for observing which areas of the surface do not contain uniformity. For example, a pair of consecutive scans are shown below for a Pd-sputtered PTFE surface in air. Since the two scans were run in sequence, they should represent the same topography. In Figure 37 an object is clearly visible on the left edge of the surface of both scans, most likely representative of an impurity that was not removed during rinsing. It can be assumed that an impurity on the surface would not have the same composition as the surface, and so should also be visible in the phase shift image. This is shown in Figure 38, where the increased phase shift in the same region clearly outlines the impurity.

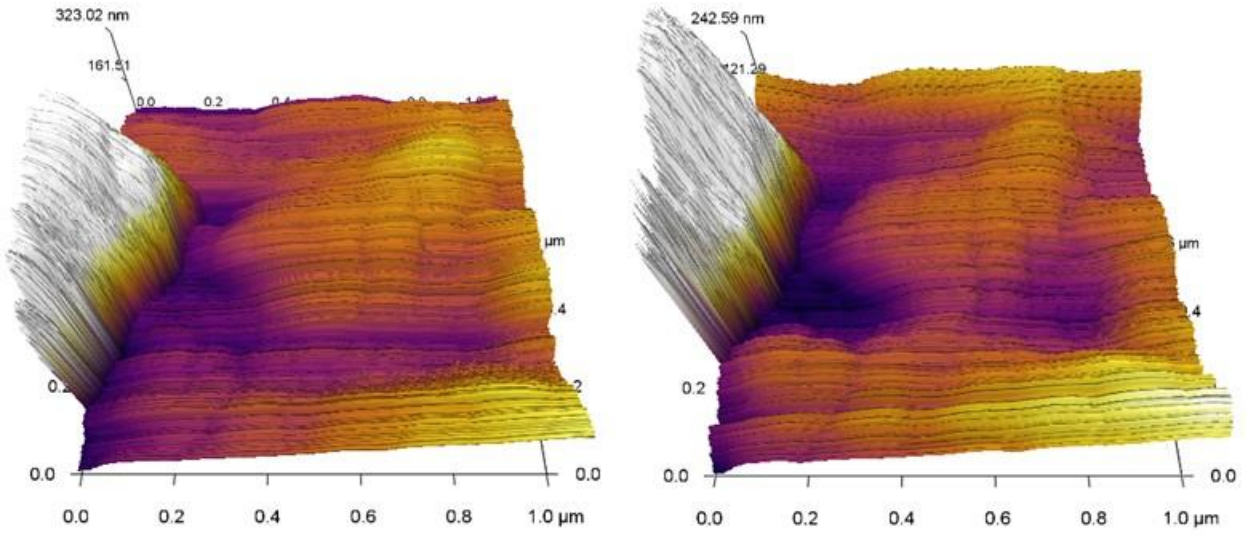

Figure 37. Sequential scans in air of a Pd-sputtered PTFE surface. An impurity on the surface is clearly represented by the rise in topography on the left side of both scans.

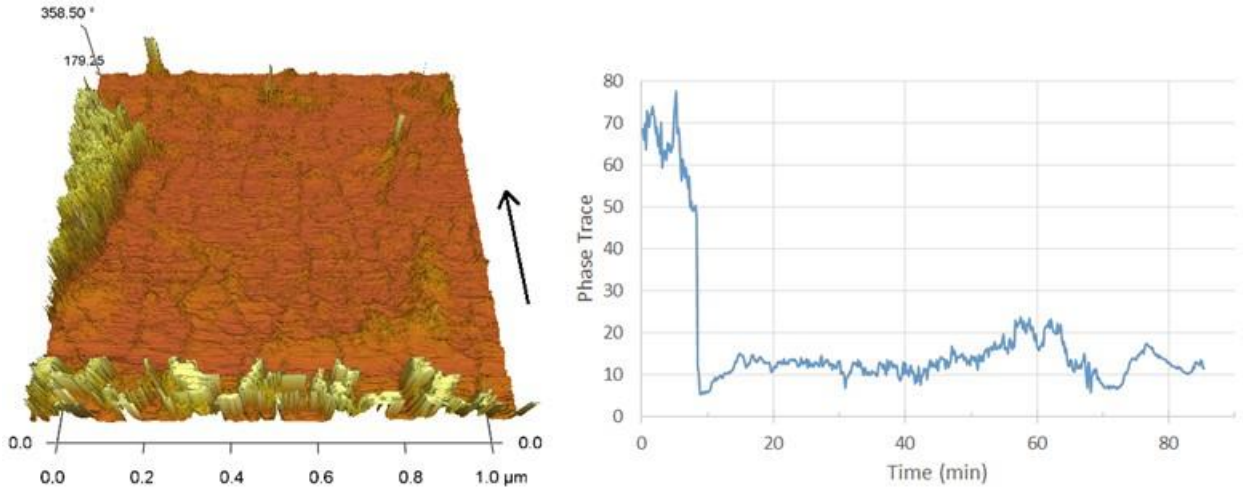

Figure 38. Phase trace image of the surface from Figure 37 and respective 2D line average plot. The shape of the impurity is clearly outlined in the image on the left, indicating that the impurity surface interacts differently with the probe than the sample surface. The presence of the impurity is less noticeable in the 2D plot.

The consequence of this impurity is shown in the line-averaged 2D plot of phase trace vs time, where the higher phase trace values of the impurity raise the respective line average. Left unnoticed, the impurity could cause false conclusions about the system to be drawn from errors in the phase data, especially if the location of the impurity were to coincide with intentional system changes such as gas switching or reagent injection. There are two ways to reduce any error caused by impurities on the surface, which can also be used for noise in the data:

- Compare the 3D plot to the 2D line average, and simply ignore any trends or changes taking place in areas of noise or obvious impurity.
- Observe the 3D plot for areas of noise or impurity and remove those sections of data from the spreadsheet prior to performing line averaging.

6.1 Impact of probe geometry

Atomic force microscopy can provide extremely high-resolution images, but there are still limitations due to the physical dimensions of the tip of the probe. Figure 39 below shows the geometry of the cantilever used for liquid scans. Since the sputtered palladium layer is only ~12 nm thick and the area of the scan is just 1.0 μm^2, the 3.5 μm long probe itself is very large by comparison. However, the diameter of the tip is 16 nm. Features smaller than the probe tip would not be able to be clearly resolved in the topography or phase image, and the tip may cause other data anomalies when contacting features of similar size. Were the tip to oscillate over a 20-nm wide well-shaped gap with some measurable depth, the compression of the fluid inside the well may result in the tip interacting strongly with the fluid rather than the sample surface. Similarly, if the tip were to be physically restrained by the frictional forces from the sides of the well, this could also result in changes in the phase trace data. This phenomenon has been observed in multiple scans, and the phase trace tends to increase in the presence of these small valleys.

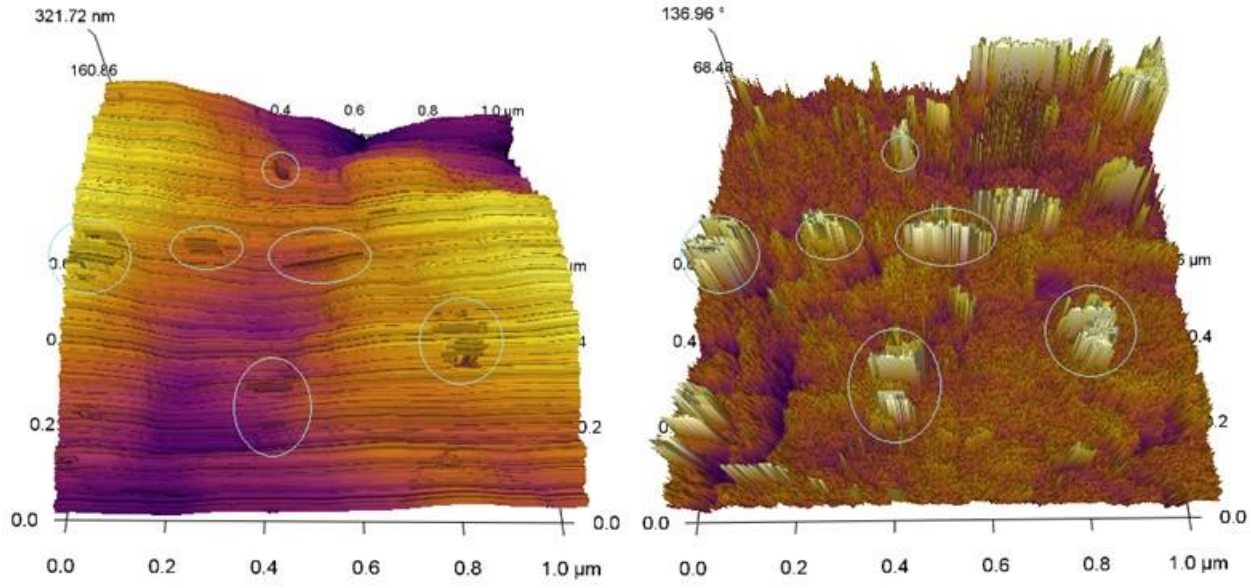

Figure 39. 3-D images of topography (left) and phase (right) for a specific scan of a palladium surface in liquid. The trenches shown in the topography image correlate to positive spikes in phase trace. The most easily visible cases have been circled for observation.

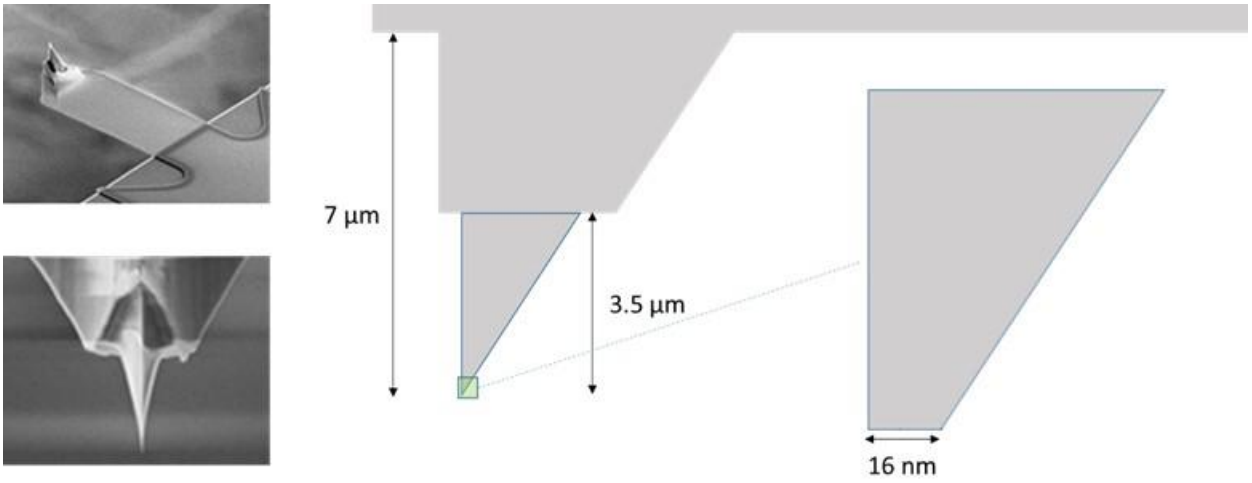

Figure 40. Cantilever geometry BL-AC40TS liquid tip.

7 Conclusions

A catalytic membrane reactor (CMR) system has been used to perform the catalytic hydrogenation of phenylacetylene to ethylbenzene on a Pd-sputtered, nonporous PTFE film at room temperature and atmospheric pressure. These conditions allow for the catalyst surface to be observed in real time by AFM. The final hydrogenation product, ethylbenzene, has been identified in the bulk fluid by GC. It has been determined that with a calculated H_2 molar flow rate of $3.7 \cdot 10^{-9}$ mol/s and a theoretical required H_2 molar flow rate of $2.3 \cdot 10^{-7}$ mol/s, the reaction in the CMR system is hydrogen starved. Based on the CMR results, styrene, the first hydrogenation product in the two-stage hydrogenation, was later used as the bulk liquid reactant in place of phenylacetylene during AFM scanning to simplify the process to a single reaction and reduce the hydrogen demand. It has been shown that it is possible to use phenylacetylene as a liquid scanning medium for AFM, and methods to account for changes in fluid temperature and thermal

motion have been presented. A more robust tuning procedure has been developed to help alleviate noise when scanning in liquid. The addition of ethylbenzene into an ethylbenzene immersed AFM scan does not have a significant effect on the 2-D line averaged plot of the phase trace other than those caused briefly by physical agitation. The addition of ethylbenzene into a styrene-immersed AFM appears to cause a decrease in phase which simulates the expected change during hydrogenation, though more data needs to be gathered.

Detection of the onset of a liquid phase hydrogenation on a catalytic surface has for the first time been detected by observing the phase shift of AFM. Styrene will cause an increase in the phase trace when added to an ethylbenzene-immersed scan on a palladium surface with hydrogen supplied to the catalyst surface by diffusion from the bulk palladium below, due to the interaction between styrene and activated hydrogen.

8 Recommendations and Outlook

8.1 Further Interpretation of AFM Data

The process for performing AFM scans under liquid has been improved upon, and the next step is to gather a greater volume of data to observe and confirm specific trends related to hydrogenation.

8.2 Increasing Hydrogen Availability

Since each point in the 2D plot of phase trace consists of an averaging of many data points, small changes in the phase trace can be obscured by noise in the system or by the nature of averaging a large volume of data points. This may be exacerbated in a CMR hydrogenation system that progresses very slowly. If the reaction is limited by hydrogen availability, increasing the supply of hydrogen could potentially increase the resolution of the phase trace data. If the reaction progresses fast enough, higher conversion could be achieved on a time scale that is reasonable for

the duration of an AFM scan. This could be made possible using a porous support layer rather than a dense PTFE film. Composite films or asymmetric polymeric membranes could provide an alternative sample surface for the sputter coating of a catalyst film layer. Various materials would need to be explored to ensure that the support is insoluble in the scanning medium.

8.3 Effects of Catalyst Morphology on Surface Hydrogen Availability

Changing from a single, defect-free Pd layer to a different catalyst morphology is not experimentally difficult, but could provide interesting data during AFM analysis. From Figure 41 below, there are three potential pathways by which hydrogen could interact with the surface:

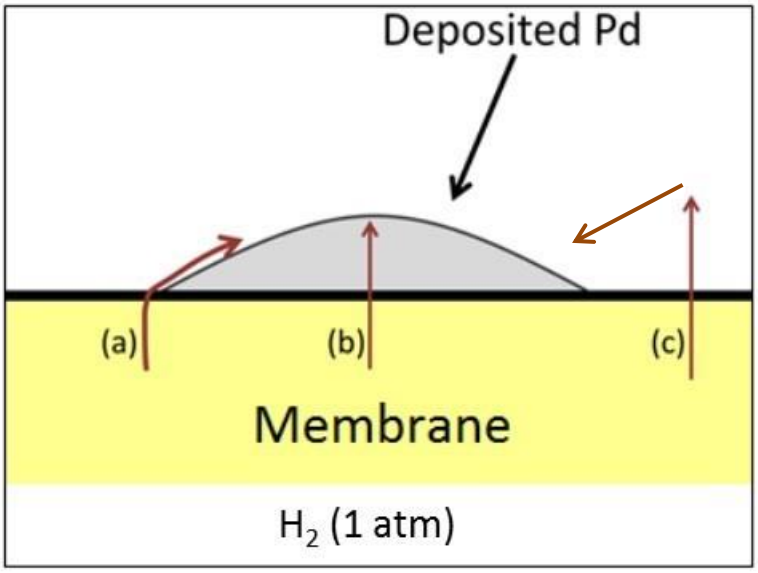

Figure 41. Expected potential mass transfer paths for hydrogen.

a) Hydrogen interacts with the Pd catalyst at the outer metal/polymer interface and diffuses over the surface of the catalyst.
b) Hydrogen diffuses through the entire catalyst, appearing at the surface.
c) Hydrogen diffuses through the membrane and does not interact with the catalyst, diffusing instead into the bulk fluid, and then diffuses back down to the catalyst.

Each pathway is possible, but diffusion limitations will vary the time at which they can occur. Path (a) is likely fastest due to no diffusion occurring through the metal catalyst or the bulk fluid. Path (b) requires the diffusion of hydrogen through the solid Pd, which is a function of catalyst thickness. Path (c) requires the hydrogen to dissolve into the fluid and diffusing to the surface of the catalyst. Catalyst morphology, surface coverage, solubility, and diffusion coefficients all govern the transport mechanism. The data provided by AFM can possibly provide insight as to the most optimal configuration for improving hydrogen availability at the catalyst surface.

8.4 Scanning under realistic reaction conditions using improved AFM system

A more sophisticated atomic force microscope has been developed for use at elevated temperatures and pressures, and is capable of reaching 360 K and 100 atm, respectively [45]. This allows for the use of AFM scanning at realistic reaction conditions and opens up a much wider range of potential reactions to choose for observation.

8.5 Quantifying the styrene-immersed system using phase trace data

Based on work conducted in the gas phase [21, 46], it is possible to determine the phase trace shift of varied materials in a heterogeneous system. By observing and quantifying the change in phase trace caused by the conversion of styrene to ethylbenzene, or the introduction of styrene to an ethylbenzene immersed scan as performed here, it may be possible to define the Young's Modulus and other experimental parameters of the system.

9 Appendix

9.1 Troubleshooting an erratic sum signal

During scans of the catalyst surface in air, it was noticed that rather than the Sum signal remaining constant, it fluctuated erratically. These fluctuations occurred before and after tuning, and both during scanning and while stationary. After contacting Asylum Research, it was suggested to test the high voltage (HV) and low voltage (LV) DC power supply contacts with an oscilloscope to check for AC ripple. AC ripple is a residual periodic variation of the DC power supply caused by incomplete smoothing of the alternating waveform from the AC source.

The high voltage and low voltage DC contacts on the AFM control box were probed using an oscilloscope (model, SN). It was believed that the AC signal from the 120V supply was not being adequately filtered from the DC supply to the AFM head. The following images were captured using the oscilloscope:

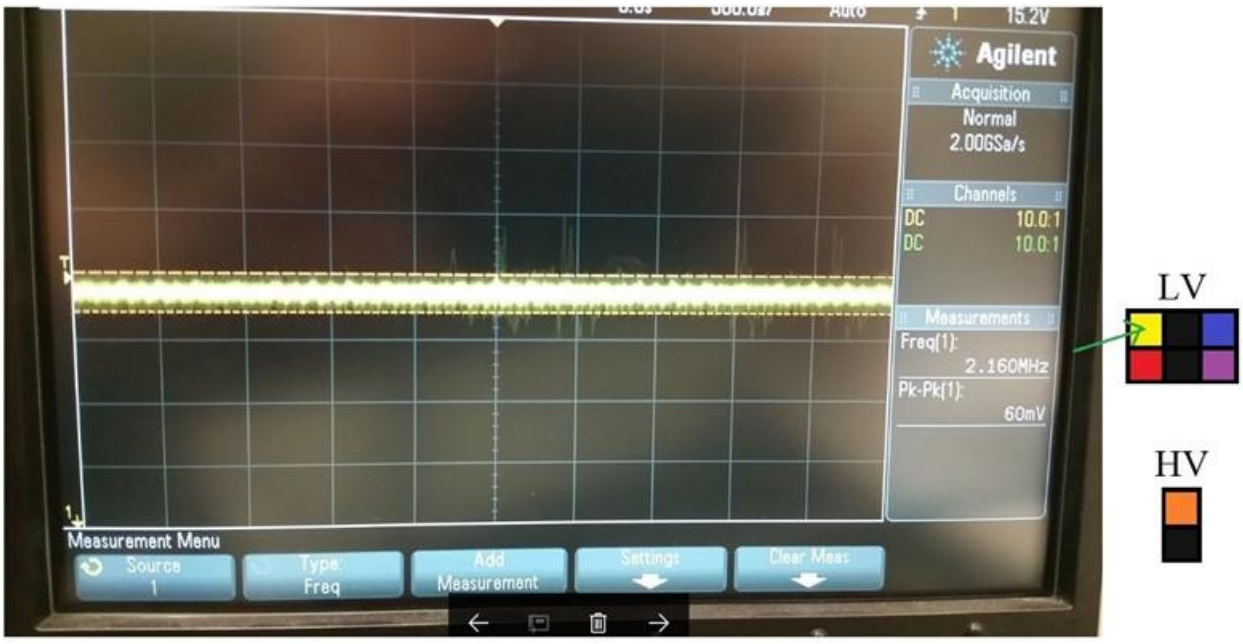

Figure 42. Oscilloscope readout displaying AC ripple from one of the Low Voltage DC power supply contacts, identified in the schematic on the right.

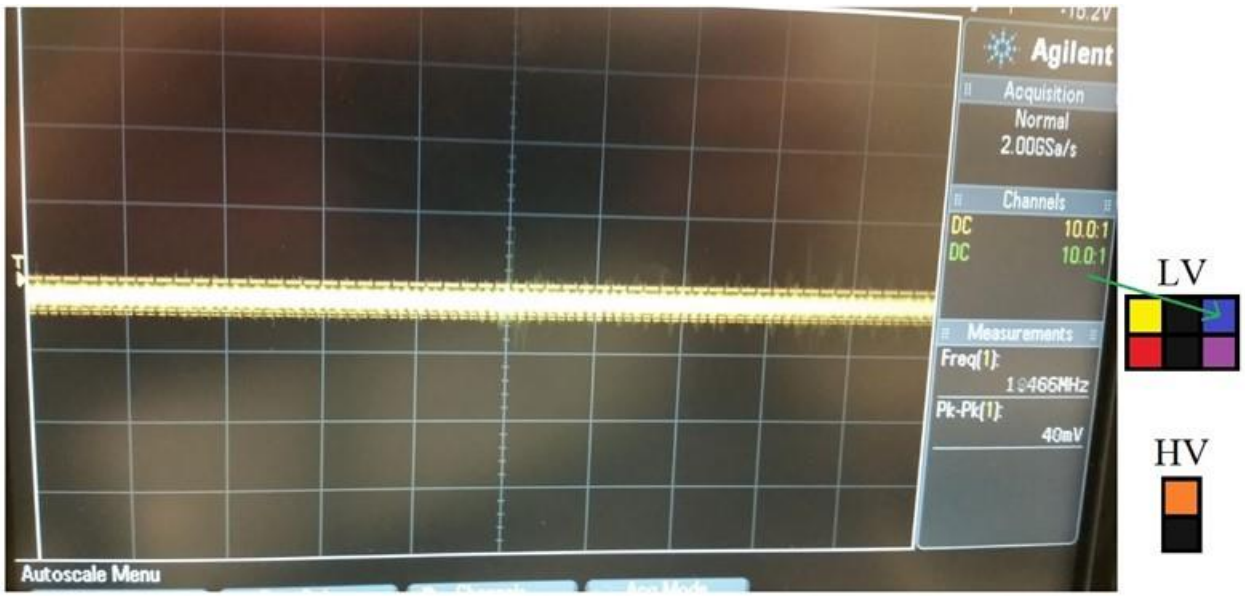

Figure 43. Oscilloscope readout displaying AC ripple from one of the Low Voltage DC power supply contacts, identified in the schematic on the right.

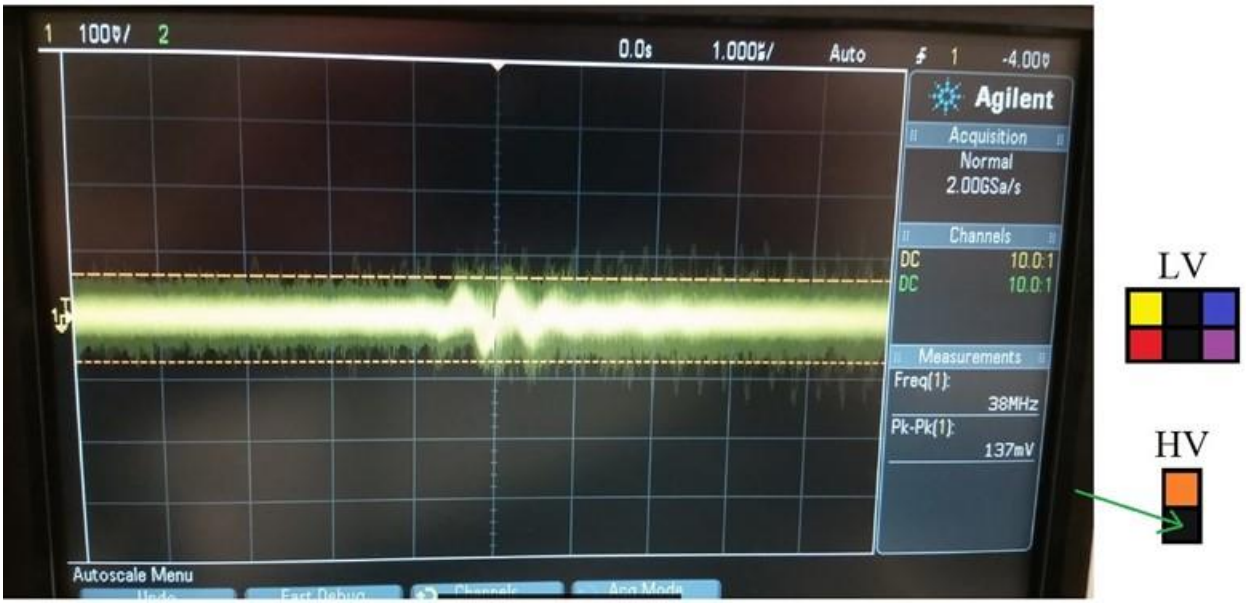

Figure 44. Oscilloscope readout displaying AC ripple from one of the High Voltage DC power supply contacts, identified in the schematic on the right.

These images confirmed an AC ripple in the DC power supply, resulting from inadequate filtering of the AC signal. This fluctuation in the power supply caused the associated fluctuation in the Sum signal during scanning. The control box was returned to Asylum Research for repair and has since been confirmed to be clear of AC ripple (verified by constant Sum signal).

Though the Sum signal is important for identifying small variations in the phase shift, the fluctuations should not have had a noticeable impact on the topography images, since those are developed from a physical interaction between the cantilever tip and the sample surface. It is possible that the resolution of the images could have been affected, but no significant change in topography resolution was observed between scans before the Sum signal fluctuation was first discovered.

9.2 Raw Phenylacetylene Hydrogenation GC Data

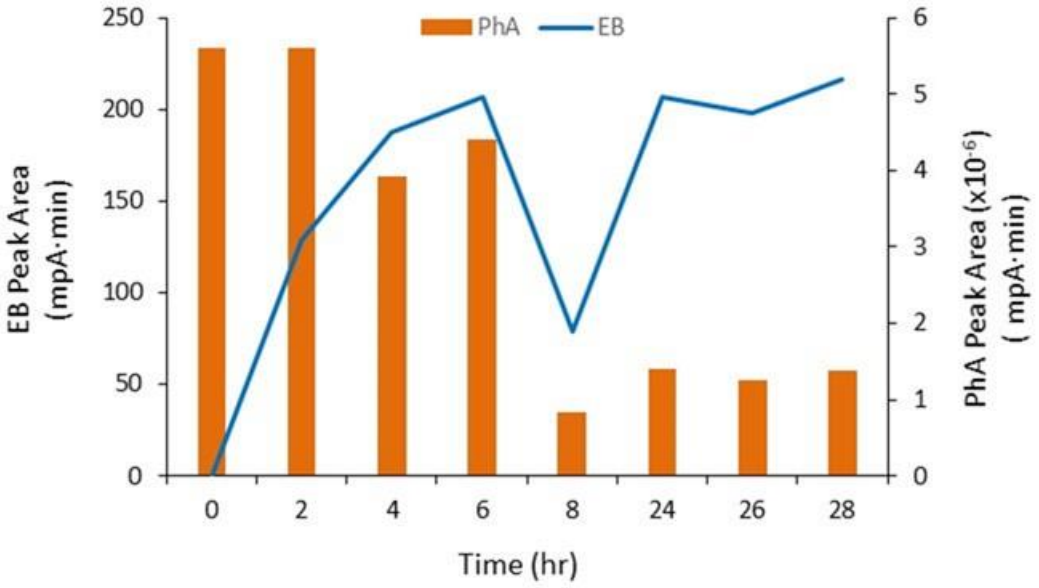

Figure 45. Plot of absolute PhA and EB peak area as a function of time.

The EB peak area (line), when viewed alone can appear to follow a generally increasing trend which eventually stabilizes, except for an outlying data point at hour 8. However, when compared to the plot of the PhA peak area (columns), which should be approximately constant across samples of equal volume, the data becomes much more difficult to interpret. The wide variation from one sample to the next reflects the GC sensitivity to small changes in sample volume and manual injection consistency, highlighting the need for a normalization across the samples.

9.3 Photographs of AFM Setup

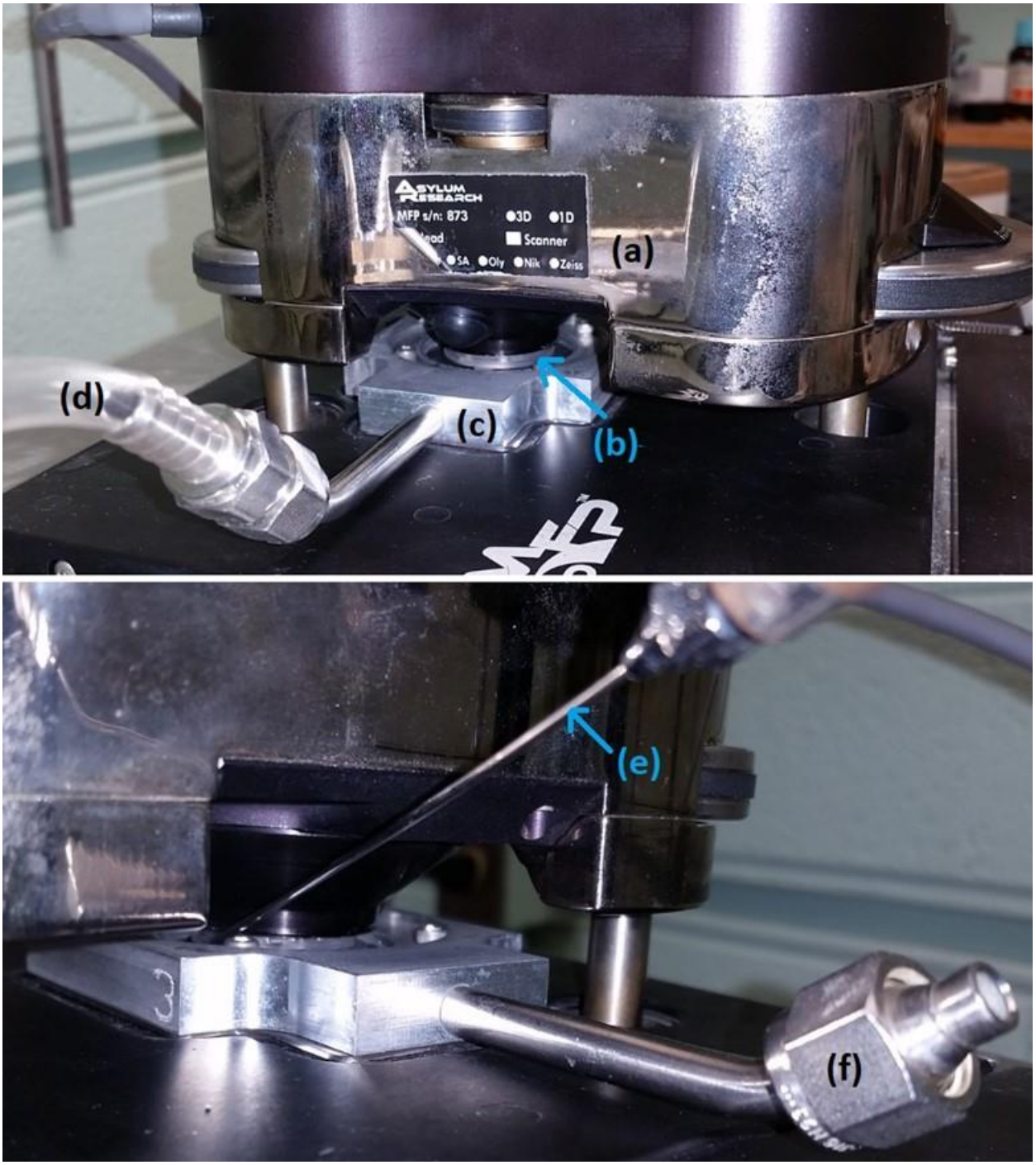

Figure 46. Photographs of the AFM lab setup (top) and injection (bottom). Identified in the image are the AFM head (a), cantilever holder (b), sample holder (c), gas supply line (d), extended injection needle (e), and the gas outlet (f).

9.4 Discarded Phase Plots

9.4.1 Palladium Immersed in Ethylbenzene with Gas Switching

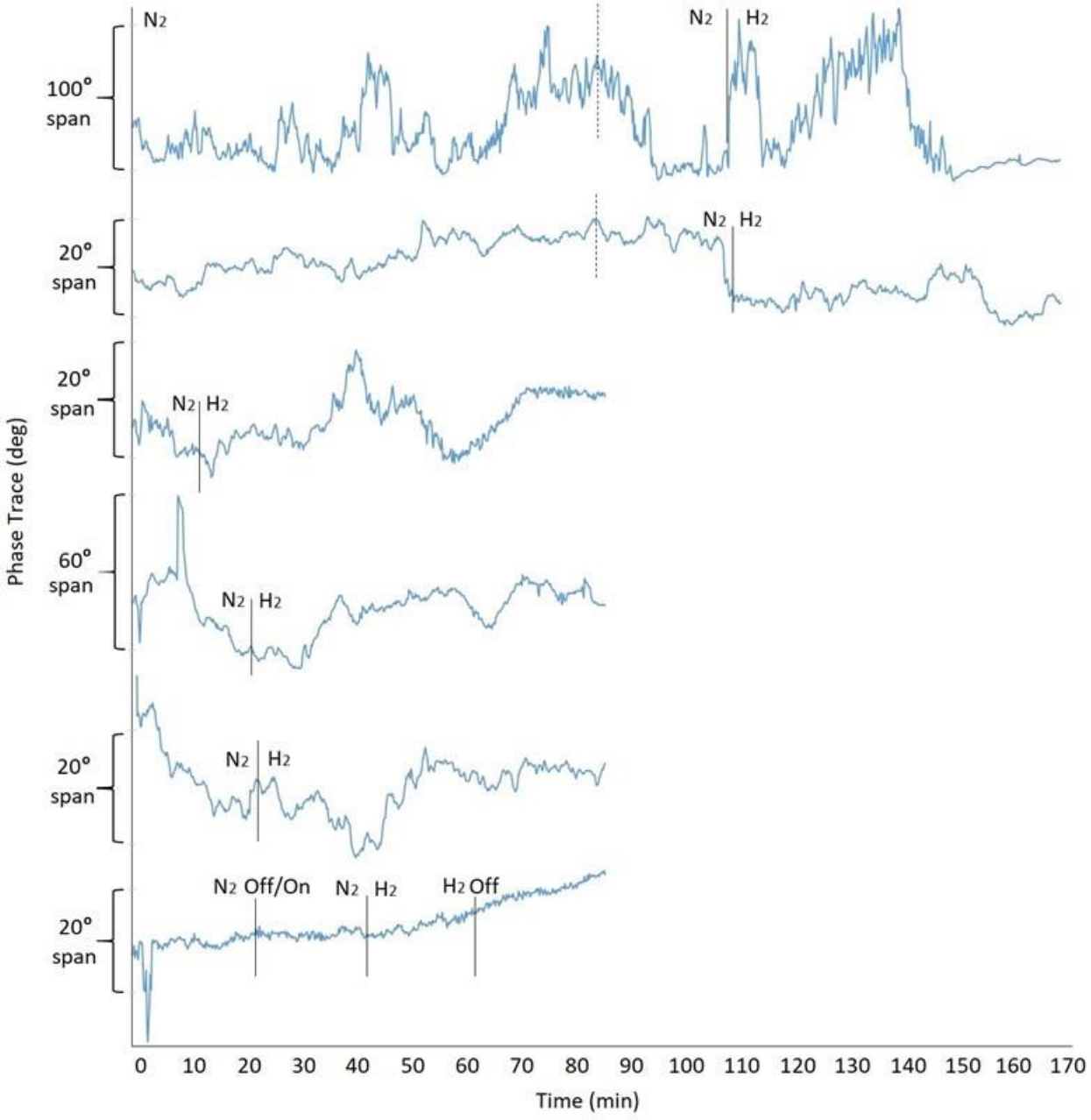

Figure 47. Assorted line-averaged AFM phase plots for a Pd-sputtered PTFE film immersed in ethylbenzene with changes in the supplied gas.

9.4.2 Palladium Immersed in Styrene with Injections

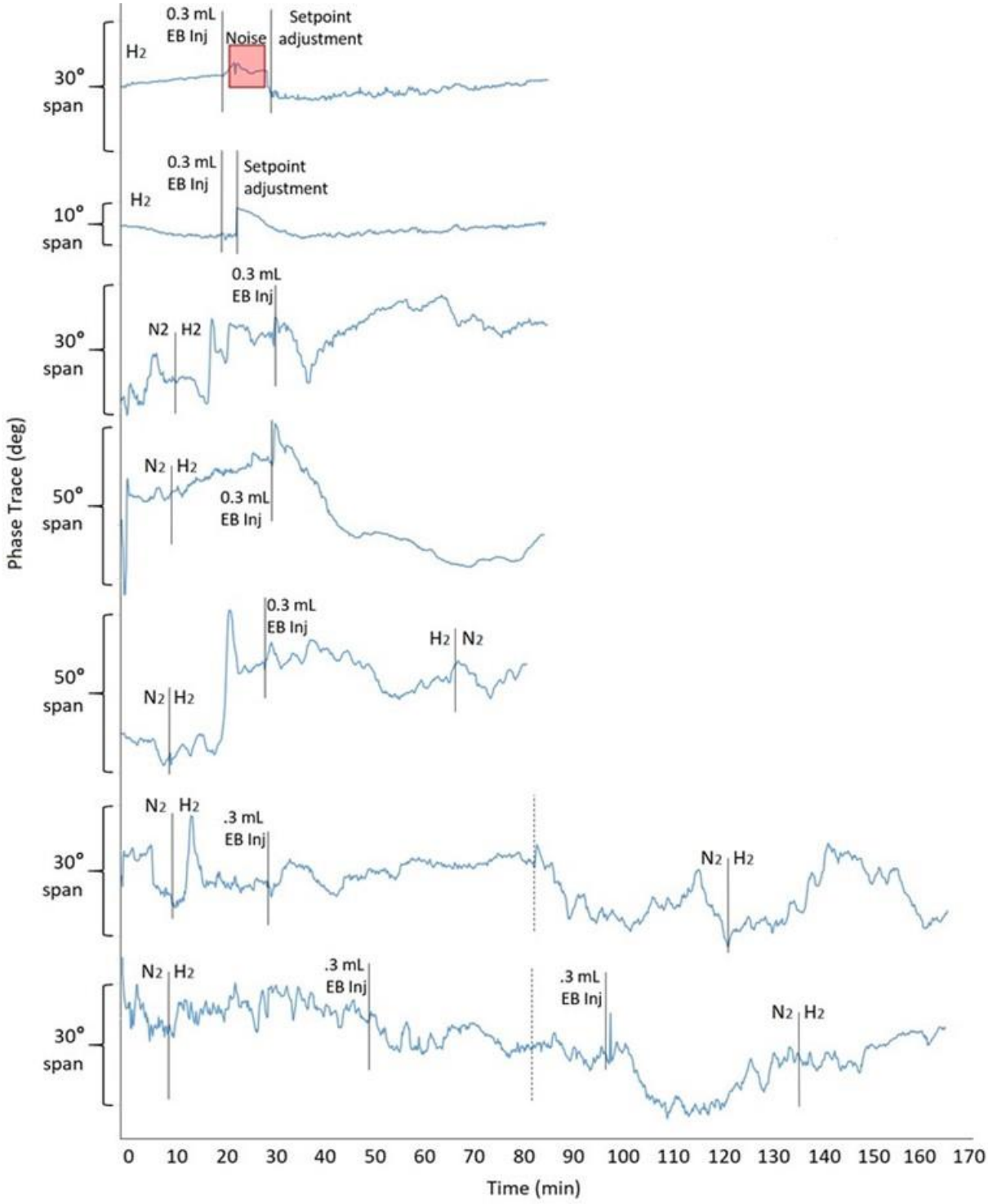

Figure 48. Assorted line-averaged AFM phase plots for a Pd-sputtered PTFE film immersed in styrene with changes in the supplied gas and injections of ethylbenzene.

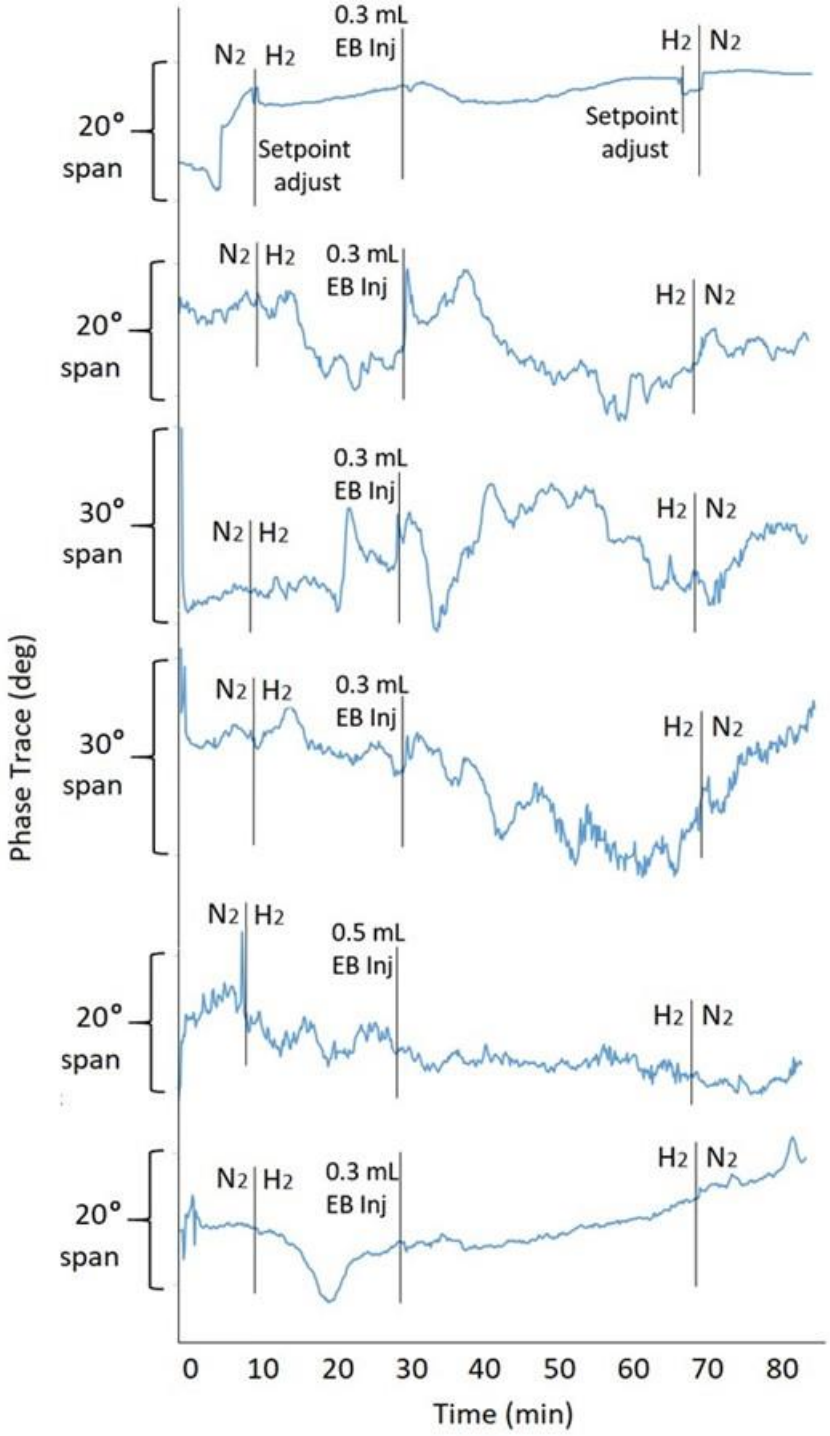

Figure 49. Assorted line-averaged AFM phase plots for a Pd-sputtered PTFE film immersed in styrene with changes in the supplied gas and injections of ethylbenzene.

9.4.3 Palladium Immersed in Ethylbenzene with Injections

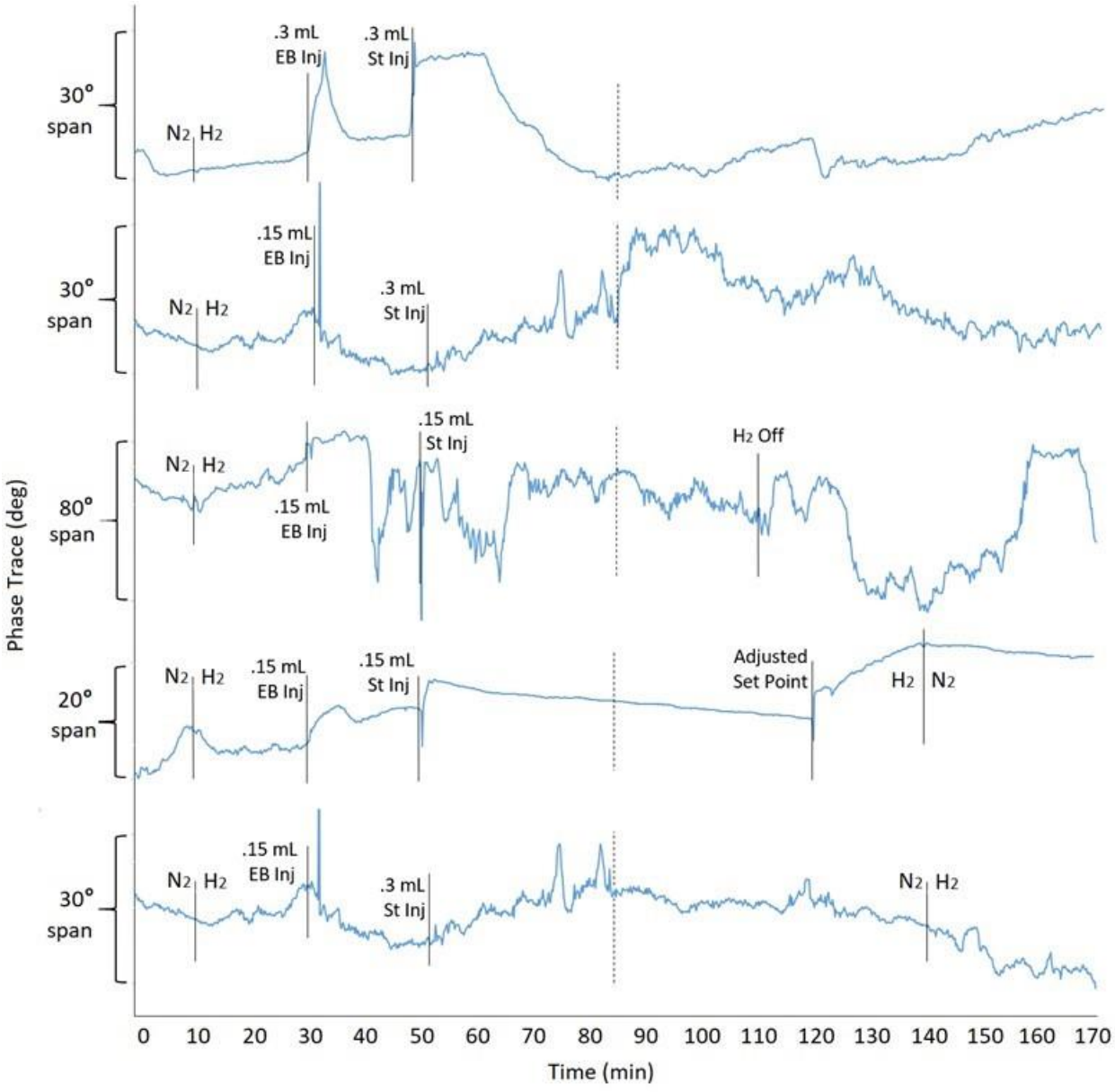

Figure 50. Assorted line-averaged AFM phase plots for a Pd-sputtered PTFE film immersed in ethylbenzene with changes in the supplied gas and injections of ethylbenzene and styrene.

10 References

[1] R. Noyori, "Synthesizing Our Future," *Nature Chemistry,* vol. 1, no. 1, pp. 5-6, 2009.

[2] Johnson Matthey Plc, "Platinum 2013," *Platinum Metals Rev.,* vol. 57, no. 3, p. 215, 2013.

[3] J. R. H. Ross, Heterogeneous Catalysis: Fundamentals and Applications, Oxford, U.K.: Elsevier, 2011, p. 172.

[4] D. Singh,, M. E. Rezac and P. H. Pfromm, "Partial Hydrogenation of Soybean Oil using Metal Decorated Integral-asymmetric Polymer Membranes: Effects of Morphology and Membrane Properties," *J. Membr. Sci.,* vol. 348, pp. 99-108, 2010.

[5] U. K. Singh and M. A. Vannice, "Kinetics of Liquid-phase Hydrogenation Reactions over Supported Metal Catalysts: A Review," *Appl. Catal.,* vol. 213, pp. 1-24, 2001.

[6] A. H. Zacher, M. V. Olarte, D. M. Santosa, D. C. Elliott and S. B. Jones, "A Review and Perspective of Recent Bio-oil Hydrotreating Research," *Green Chem.,* vol. 16, pp. 491-515, 2014.

[7] A. S. Berenblyum, H. A. Al-Wadhaf and E. A. Katsman, "Supported Palladium Nanomaterials as Catalysts for Petroleum Chemistry: 2. Kinetics and Specific Features of the Mechanism of Selective Hydrogenation of Phenylacetylene in the Presence of Carbon-Supported Palladium Nanocatalyst," *Petroleum Chemistry,* vol. 55, no. 2, pp. 118-126, 2015.

[8] G. Fagherazzi, A. Benedetti, G. Deganello, D. Duca, A. Martorana and G. Spoto, "Pumice-Supported Palladium Catalysts I. Chemical Preparation and Microstructural Features," *Journal of Catalysis,* vol. 150, pp. 117-126, 1994.

[9] D. Duca, L. F. Liotta and G. Deganello, "Selective Hydrogenation of Phenylacetylene on Pumice-Supported Palladium Catalysts," *J. Catal.,* pp. 69-79, 1994.

[10] J. W. B. Veldsink, M. J. Schoon, N. H. Beenackers and A. C. M. Antonie, "Heterogeneous hydrogenation of vegetable oils: a literature review," *Catal. Rev. Sci. Eng.,* vol. 39, pp. 253-318, 1997.

[11] I. Horiuti and M. Polanyi, "Exchange reactions of hydrogen on metallic catalysts," *Trans. Faraday Soc.,* vol. 30, pp. 1164-1172, 1934.

[12] R. Guettel, U. Kunz and T. Turek, "Reactors for Fischer-Tropsch Synthesis," *Chem. Eng. Technol.,* vol. 31, no. 5, pp. 746-754, 2008.

[13] J. Shu, B. P. A. Grandjean, A. Van Neste and S. Kaliaguine, "Catalytic Palladium-based Membrane Reactors: A Review," *Can. J. Chem. Eng.,* vol. 69, pp. 1036-1060, 1991.

[14] W. R. Baker, "Future Directions of Membrane Gas Separation Technology," *Ind. Eng. Chem. Res.,* vol. 41, no. 6, pp. 1393-1411, 2002.

[15] J. Peureux, M. Torres, H. Mozzanega, A. Giroir-Fendler and J.-A. Dalmon, "Nitrobenzene liquid-phase hydrogenation in a membrane reactor," *Catal. Today,* vol. 25, no. 3-4, pp. 409-415, 1995.

[16] F. Zaera, "Probing Liquid/Solid Interfaces at the Molecular Level," *Chem. Rev.,* vol. 112, pp. 2920-2986, 2012.

[17] J. Broekmaat, A. Brinkman, D. H. A. Blank and G. Rihnders, "High temperature surface imaging using atomic force microscopy," *Appl. Phys. Lett.,* vol. 92, no. 4, 2008.

[18] S. B. Roobal, M. E. Cañas-Ventura, M. Bergman, M. A. van Spronsen, W. G. Onderwaater, P. C. van der Tuijn, R. Koehler, A. Ofitserov, G. J. C. van Baarle and J. W. M. Frenken, "The ReactorAFM: Non-contact atomic force microscope operating under high-pressure and high-temperature catalytic conditions," *Rev. Sci. Instrum.,* vol. 86, no. 3, 2015.

[19] D. Rugar and P. Hansma, "Atomic Force Microscopy," *Phys Today,* vol. 43, no. 10, pp. 23-30, 1990.

[20] V. J. Morris, A. R. Kirby and A. P. Gunning, Atomic Force Microscopy for Biologists, 2nd Ed., London: Imperial College Press, 2010.

[21] M. J. Young, "Studying Liquid-Phase Heterogeneous Catalysis Using the Atomic Force Microscope," Ph.D. dissertation, Dept. Chem. Eng., Kansas State Univ., Manhattan, 2016.

[22] M. J. Young, P. H. Pfromm, M. E. Rezac and B. M. Law, "Analysis of Atomic Force Microscopy Phase Data To Dynamically Detect Adsorbed Hydrogen Under Ambient Conditions," *Langmuir,* vol. 30, pp. 11906-11912, 2014.

[23] M. J. Young, J. C. Carson, P. H. Pfromm, M. E. Rezac and B. M. Law, "Atomic Force Phase Imaging for Dynamic Detection of Adsorbed Hydrogen on a Catalytic Palladium Surface under Liquid," *(In Review),* 2016.

[24] D. Duca, L. F. Liotta and G. Deganello, "Selective Hydrogenation of Phenylacetylene no Pumice-Supported Palladium Catalysts," *J. Catal.*, pp. 69-79, 1994.

[25] W. Liu, C. O. Arean, S. Bordiga, E. Groppo and A. Zecchina, "Selective Phenylacetylene Hydrogenation on a Polymer-Supported Palladium Catalyst Monitored by FTIR Spectroscopy," *ChemCatChem,* vol. 3, pp. 222-226, 2011.

[26] Z. Wang, L. Yang, L. Li, Z. Cheng and Z. Zhou, "Slective hydrogenation of phenylacetylene over bimetallic Pd-Cu/Al2O3 and Pd–Zn/Al2O3 catalysts," *Catal. Today*, vol. 264, pp. 37-43, 2016.

[27] S. D. Jackson and L. A. Shaw, "The liquid-phase hydrogenation of phenyl acetylene and styrene on a palladium/carbon catalyst," *Appl. Catal., A,* vol. 134, no. 1, pp. 91-99, 1996.

[28] T. Vergunst, F. Kapteijn and J. A. Moulijn, "Optimization of Geometric Properties of a Monolithic Catalyst for the Selective Hydrogenation of Phenylacetylene," *Ind. Eng. Chem. Res.,* vol. 40, pp. 2801-2809, 2001.

[29] B. A. Wilhite, M. J. McCready and A. Varma, "Kinetics of Phenylacetylene Hydrogenation over Pt/γ-Al2O3 Catalyst," *Ind. Eng. Chem. Res.,* vol. 41, pp. 3345-3350, 2002.

[30] P. Weerachawanasak, O. Mekasuwandumrong, M. Arai, S.-I. Fujita, P. Praserthdam and J. Panpranot, "Effect of strong metal–support interaction on the catalytic performance of

Pd/TiO2 in the liquid-phase semihydrogenation of phenylacetylene," *J. Catal.*, vol. 262, no. 2, pp. 199-205, 2009.

[31] F. B. Bizhanov, S. D. Dinasylova and D. V. Sokolskii, "Kinetics and Mechanism of Phenylacetylene Hydrogenation Under Hydrogen Pressure," *React. Kinet. Catal. Lett.*, vol. 12, no. 3, pp. 291-296, 1979.

[32] F. A. Carey, Organic Chemistry 4th Edition, New York City: McGraw-Hill, 2000.

[33] Operating Instructions for Denton Vacuum, LLC DESK II Cold Sputter/Etch Unit and Carbon Evaporation Accessory, Moorestown, NJ: Denton Vacuum, LLC, 1998.

[34] C. San Marchi, "Technical Reference on Hydrogen Compatibility of Materials," Sandia National Laboratories, Livermore, CA, 2013.

[35] U. Hironori, N. Tatsuo and U. Isamu, "Electrochemical Measurements of Single Particles of Pd and LaNi5 with a Microelectrode Technique," *J. Electroanal. Chem.*, vol. 396, pp. 169-173, 1995.

[36] A. M. Brass and J. Collet-Lacoste, "The Influence of Surface on the Permeation of Hydrogen in Iron and Palladium," in *Proceedings of the Symposium on Electrochemical Surface Science of Hydrogen Adsorption and Absorption*, Pennington, NJ, 1997.

[37] F. J. Ackerman and G. J. Koskinas, "Permeation of Hydrogen and Deuterium Through Palladium-Silver Alloys," *J. Chem. Eng. Data*, vol. 17, no. 1, pp. 51-55, 1972.

[38] Operating Instructions for Denton Vacuum, LLC DESK II Cold Sputter/Etch Unit and Carbon Evaporation Accessory, Moorestown, NJ: Denton Vacuum, LLC, 1998.

[39] Sigma-Aldrich, "Phenylacetylene," Sigma-Aldrich, 2017. [Online]. Available: http://www.sigmaaldrich.com/catalog/product/aldrich/117706?lang=en&region=US. [Accessed 11 February 2017].

[40] Sigma-Aldrich, "Ethylbenzene," Sigma-Aldrich, 2017. [Online]. Available: http://www.sigmaaldrich.com/catalog/product/sial/296848?lang=en&region=US. [Accessed 11 February 2017].

[41] R. L. Grob and E. F. Barry, Modern Practice of Gas Chromatography, New York City: John Wiley & Sons, 2004.

[42] Z. Ke, G. Huiyuan, R. Zebao, L. Yuesheng and L. Yongdan, "Preparation of Thin Palladium Composite Membranes and Application to Hydrogen/Nitrogen Separation," *J. Chem. Eng.*, pp. 643-647, 2007.

[43] S. B. Roobol, M. E. Canas-Ventura, M. Bergman, M. A. van Spronsen, W. G. Onderwaater, P. C. van der Tuijn, R. Koehler, A. Ofitserov, G. J. C. van Baarle and J. W. M. Frenken, "The Reactor AFM: Non-contact atomic force microscope operating under high-pressure and high-temperature catalytic conditions," *Rev. Sci. Instrum.*, p. 86, 2015.

[44] R. A. Pasternak, M. V. Christensen and J. Heller, "Diffusion and Permeation of Oxygen, Nitrogen, Carbon Dioxide, and Nitrogen Dioxide through Polytetrafluoroethylene," *Macromolecules*, vol. 3, no. 3, pp. 366-371, 1969.

[45] A. S. Lea, S. R. Higgins, K. G. Knauss and K. M. Rosso, "A high-pressure atomic force microscope for imaging in supercritical carbon dioxide," *Rev. Sci. Instrum.*, vol. 82, no. 4-043709, pp. 1-7, 2011.

[46] Y. Zhao, Q. Cheng, M. Qian and J. H. Cantrell, "Phase image contrast mechanism in intermittent contact atomic force," *J. Appl. Phys.*, vol. 108, p. 094311, 2010.

[47] R. W. Bowen and N. Hilal, Atomic Force Microscopy in Process Engineering: Introduction to AFM for Improved Processes and Products, Burlington, MA: Elsevier, 2009.